Chemical Geology 517 (2019) 7–21

Contents lists available at ScienceDirect

Chemical Geology

journal homepage: www.elsevier.com/locate/chemgeo

Implications of nano- and micrometer-size platinum-group element minerals in base metal sulfides of the Yangliuping Ni-Cu-PGE sulfide deposit, SW China

Qing-Lin Liang[a,b], Xie-Yan Song[a,*], Richard Wirth[c], Lie-Meng Chen[a], Zhi-Hui Dai[a]

[a] State Key Laboratory of Ore Deposit Geochemistry, Institute of Geochemistry, Chinese Academy of Sciences, Guiyang, PR China
[b] University of Chinese Academy of Sciences, Beijing 100039, China
[c] German Research Centre for Geosciences GFZ, 3.5 Surface Geochemistry, Telegrafenberg, Potsdam, Germany

ARTICLE INFO

Editor: D.B. Dingwell

Keywords:
Nanometer-size PGE-arsenides and sulfarsenides
Semimetal elements
Pt-As molecular
PGE distribution

ABSTRACT

The concentrations of platinum-group elements (PGE) and semimetal elements (As, Sb, Se, Te and Bi) in the base metal sulfides from the Yangliuping deposit were determined using Laser Ablation Inductively Coupled Plasma Mass Spectrometry (LA-ICPMS). Mass balance calculation reveals that the base metal sulfides only contain < 40 wt% Os, < 15 wt% Ir, < 25 wt% Pd and negligible Pt, Rh and As, as solid solution. Such PGE percentages in the base-metal sulfides as solid solution are evidently lower than in the sulfides from the Jinchuan, Noril'sk and Sudbury Ni—Cu-(PGE) sulfide deposits. Euhedral shape and similar chemical composition of the nanometer-size PGE-arsenides and sulfarsenides in the base-metal sulfides suggest that they crystallized from the sulfide melt before the crystallization of monosulfide solid solution (MSS) and intermediate solid solution (ISS). It is proposed that the nanometer-size PGE-arsenides and sulfarsenides formed from PGE-As molecular or polymolecular clusters in the sulfide liquid at high temperature. The PGE-As molecular or polymolecular clusters prevent As and PGE from partitioning into the base metal sulfide lattice and tend to form discrete nanometer-size PGE-arsenides and sulfarsenides. Thus, semimetal elements, particularly As, play an important role on behaviour of PGE during solidification of magmatic sulfide liquids.

1. Introduction

Platinum-group elements (PGE) are usually present in the ng/g up to the μg/g level in magmatic sulfide deposits (Cabri and Laflamme, 1976; Barnes et al., 2006; Godel et al., 2010). It is well known from experimental and empirical studies that IPGE (Os, Ir, Ru) and Rh tend to partition into monosulfide solid solution (MSS), whereas Pt and Pd behave incompatible and concentrate in the residual sulfide liquid, from which intermediate solid solution crystalizes (Barnes et al., 1997; Barnes et al., 2001; Brenan, 2002; Prichard et al., 2004; Mungall et al., 2005). Up on cooling, both MSS and ISS decompose to base metals sulfides; pyrrhotite, pentlandite and chalcopyrite. Even though base metal sulfides can theoretically accommodate high contents of PGE, the latter commonly form discrete phases with similarly rare semimetals (Cabri and Laflamme, 1976; Hanley, 2007). Recent studies using Laser Ablation Inductively Coupled Plasma Mass Spectrometry (LA-ICPMS) and Microparticle Induced X-ray Excitation (micro-PIXE) indicated that both pentlandite and pyrrhotite may be rich in Os, Ir, Ru and Rh, while pentlandite may be rich in Pd, whereas, chalcopyrite is usually barren in PGEs (Czamanske et al., 1992; Barnes and Maier, 1999; Barnes et al., 2006; Cabri et al., 2008; Dare et al., 2010a). It was proposed that Pd tends to enter into the pentlandite from the sulfide liquid during solid exsolution of the MSS and ISS (Cabri and Laflamme, 1976; Barnes et al., 2008). In the Noril'sk Ni—Cu-PGE sulfide deposit (Russia), > 70% IPGE and > 90% Pd are contained in BMS (Barnes et al., 2008). However, in the Jinchuan (China) and the Creighton Ni—Cu-(PGE) sulfide deposit, Sudbury (Canada), PGE are not dominantly hosted by the BMS (Dare et al., 2010a; Chen et al., 2015). On the other hand, PGE hosted by BMS are not only occurring as solid solution but also in tiny PGE-rich particles (Barnes et al., 2008; Dare et al., 2010a; Chen et al., 2015). The factors causing the large variation in the PGE concentrations contained in base-metal sulfides between different deposits are still not well addressed. Previous studies have manifested that the presence of semimetals in the sulfide melt may lead to the incorporation of Pt and Pd (and potentially the other PGEs) into semimetal-rich melts (Fleet et al., 1993; Gervilla et al., 1996; Makovicky and Karup-Møller, 2000; Helmy

* Corresponding author.
E-mail address: songxieyan@vip.gyig.ac.cn (X.-Y. Song).

https://doi.org/10.1016/j.chemgeo.2019.04.015
Received 14 October 2018; Received in revised form 4 April 2019; Accepted 13 April 2019
Available online 19 April 2019
0009-2541/

et al., 2007; Tomkins, 2010). Based on experimental studies, it is speculated that semimetal elements could selectively combine with PGE to form PGE-semimetal elements complexes in sulfide melt and even nanoparticles in undersaturated sulfide melt at high temperature (Helmy et al., 2013a, 2013b; Helmy and Bragagni, 2017; Helmy and Fonseca, 2017). PGE-semimetal selective complexing at magmatic temperatures explain the fractionation of PGE (Helmy and Bragagni, 2017).

The Yangliuping Ni—Cu-PGE deposit is the largest Ni—Cu-PGE sulfide deposit in the Permian Emeishan Large Igneous Province, SW China (Zhou et al., 2002; Song et al., 2008). Total PGE in the sulfide ores are up to 17 ppm (Table 2). Limited micrometer-size PGM, such as sperrylite ($PtAs_2$), testibiopalladite (Pd(Sb, Bi)Te), Pd melonite ((Ni,Pd)$(Te,Bi)_2$), sudburyite ((Pd, Ni)Sb), michenerite (PdBiTe), and omeiite ((Os, Ru)As_2), had been observed at the rims of pyrrhotite, pentlandite and chalcopyrite (Song et al., 2004). This study focuses on PGE concentrations and occurrences of nanometer-size PGE-arsenides and sulfarsenides in the base metal sulfide (BMS), cobaltite-gersdorffite solid solution (CGSS) using Scanning Electron Microscopy (SEM), Electron Probe Microanalyzer (EPMA) and laser Ablation Inductively Coupled Plasma Mass Spectrometry (LA-ICPMS). The results suggest that the nanometer-size arsenides and sulfarsenides of IPGE, Rh and Pt enclosed in BMS were formed earlier than crystallization of MSS. Our results testify the role of semimetal elements on PGM formation and PGE fractionation in natural sulfide melts.

2. Geological background

The Emeishan Large Igneous Province (ELIP) comprises Late Permian continental flood basalts and associated ~260 Ma mafic-ultramafic intrusions (Chung and Jahn, 1995; Xu et al., 2001; Zhou et al., 2002). The flood basalts cover an area > 0.5 million km^2, with a thickness ranging from several hundred meters to 5 km (Xu et al., 2001; Song et al., 2001). There are two types of mafic-ultramafic intrusions in the ELIP, including large layered intrusions hosting giant V—Ti magmatic ore deposits, such as Panzhihua and Hongge and small mafic-ultramafic intrusions containing Ni—Cu-(PGE) sulfide deposits (Zhong et al., 2002; Song et al., 2008, 2013). Several small mafic-ultramafic intrusions containing economic or sub-economic magmatic sulfide mineralization have been discovered in the central part of the ELIP. For example, PGE-rich reefs were discovered in wehrlite in the Jinbaoshan mafic-ultramafic sill and Ni—Cu sulfide ore bodies occurred in the wehrlite at the base of the funnel shaped Limahe mafic-ultramafic intrusion (Tao et al., 2007; Tao et al., 2008).

The Yangliuping Ni—Cu-PGE deposit is the largest magmatic sulfide deposit in the ELIP and located at the north-western corner of the igneous province. It is hosted by mafic-ultramafic sills within a dome structure consisting of Devonian-Permian strata (Fig. 1; Song et al., 2003). The Devonian strata consist of quartzite, graphite-bearing schist, mica schist, and marble. The Carboniferous strata are mainly composed of mica schist and calcareous slate. The Early Permian strata include marble with interlayers of schist and slate, which is conformably overlain by the Emeishan flood basalts. The sulfide mineralized mafic-ultramafic sills, including Yangliuping, Zhengziyanwuo, Xiezuoping, and Daqiangyanwuo, were emplaced in the Devonian schist and marble (Fig. 1). Sulfide mineralizations occur in all of the sills but economic mineralizations are only present in the Yangliuping and Zhengziyanwuo sills (Song et al., 2003, 2004). The mineralized sills are well fractionated and are up to 300 m thick, 2–4 km long (Fig. 1). They experienced intense post-magmatic alteration and greenschist-facies regional metamorphism. Both the Yangliuping and Zhengziyanwuo sills consist of serpentinite (10–200 m thick with average of 68 m), talc schist (10–220 m thick, 61 m in average), tremolite schist (~45 m thick), and altered gabbro (< 30 m thick) from the bottom to the top. The sulfide mineralization is predominantly restricted to the serpentinite, in which disseminated ores grade downward into net-textured and massive ores. In the disseminated ores, the sulfide minerals fill the spaces between pseudomorphs of cumulate olivine and pyroxene and become more abundant with depth in the sill. The massive ores mainly occur at the base of the Yangliuping sill (Song et al., 2003, 2004). There are sharp boundaries between the massive orebodies and the footwall rocks. Those mentioned above indicated that the orebodies were formed by segregation of immiscible sulfide melt and settled to the lower part of the sills (Song et al., 2003). Both massive and disseminated ore have a low Pd/Ir ratio, which is consistent with a magmatic origin (Song et al., 2004). The proven metal reserves of the deposit are ~0.5 million tonnes of Ni, ~0.17 million tonnes of Cu, and ~55 t of PGE. The average grade is 0.45 wt% Ni, 0.16 wt% Cu, and 0.5 ppm total PGE (Song et al., 2003). The massive ores have higher IPGE concentration (normalized to 100% sulfide) but lower Pd/Ir ratio than disseminated ores (Song, 2004). Emeishan flood basalts in this area normally have Pt and Pd abundances > 8 ppb, while some subunit of flood basalts shows PGE depletion with Pt and Pd concentrations lower than detection limit (0.45 ppb on average), which has been attributed to sulfide segregation at depth and the formation of the Yangliuping deposit (Song et al., 2006).

3. Sulfide mineralogy and texture

In the massive ores of the Yangliuping deposit, coarse-grained pyrrhotite (0.5–1 mm in diameter) is commonly partially surrounded by fine granular pentlandite. Flame-like pentlandite appears along fractures or edges of pyrrhotite grains. Chalcopyrite occurs as anhedral grains or a polycrystalline intergrowth associated with pyrrhotite. The proportions of pyrrhotite, pentlandite and chalcopyrite in the massive ores are about 80:15:5. In the disseminated ores, anhedral sulfide grains, 0.3 to 1 mm in diameter, fill the spaces between olivine and pyroxene pseudomorphs. The disseminated ores contain more chalcopyrite than the massive ores, and the proportions of pyrrhotite, pentlandite and chalcopyrite are about 70:10:20.

CGSS are the most common accessory sulfide mineral in the Yangliuping ores. They are mostly enclosed in pyrrhotite but also in pentlandite and chalcopyrite (Table 7), micron- and nanometer-size PGM have been found enclosed in pyrrhotite, pentlandite, chalcopyrite and CGSS (Tables 6, 7 see below).

4. Analytical methods

Whole-rock PGE concentrations of 9 samples were measured by Isotope Dilution Inductively Coupled Plasma Mass Spectrometry (ID-ICP-MS) after separation and pre-concentration by nickel fire-assay and Te precipitation. Semimetal elements were analyzed by Inductively Coupled Plasma Atomic Fluorescence Spectroscopy (ICP-AFS). Both PGE and semimetal elements were analyzed at the National Research Center of Geoanalysis, Chinese Academy of Geological Sciences. The chalcophile and semimetal elements were recalculated to 100% sulfides concentration following the procedure described by Barnes et al. (2006).

Six massive and disseminated ores from the Yangliuping deposit with high PGE concentration in 100% sulfide were selected from 15 fresh samples to be used in this study. Textural relationships between PGM and CGSS and BSM were observed using Reflected Light Microscopy and Scanning Electron Microscopy (SEM) at the Institute of Geochemistry, Chinese Academy of Sciences. Nanometer-size PGE-arsenides and sulfarsenides enclosed in pyrrhotite, pentlandite and chalcopyrite were observed using a FEI Nova NanoSEM at the Institute of Geology and Geophysics, Chinese Academy of Sciences. The chemical composition of CGSS was determined at Nanjing university using a JEOL JXA-8100 Electron Probe Microanalyzer (EPMA) with a beam diameter of 1 μm, the accelerating voltage was 15 kv, the beam current was 20 nA. The counting time on peak and backgrounds were 10 s and 5 s for S, Fe and As, 20 s and 10 s for other elements. Pure metal (Ir, Rh,

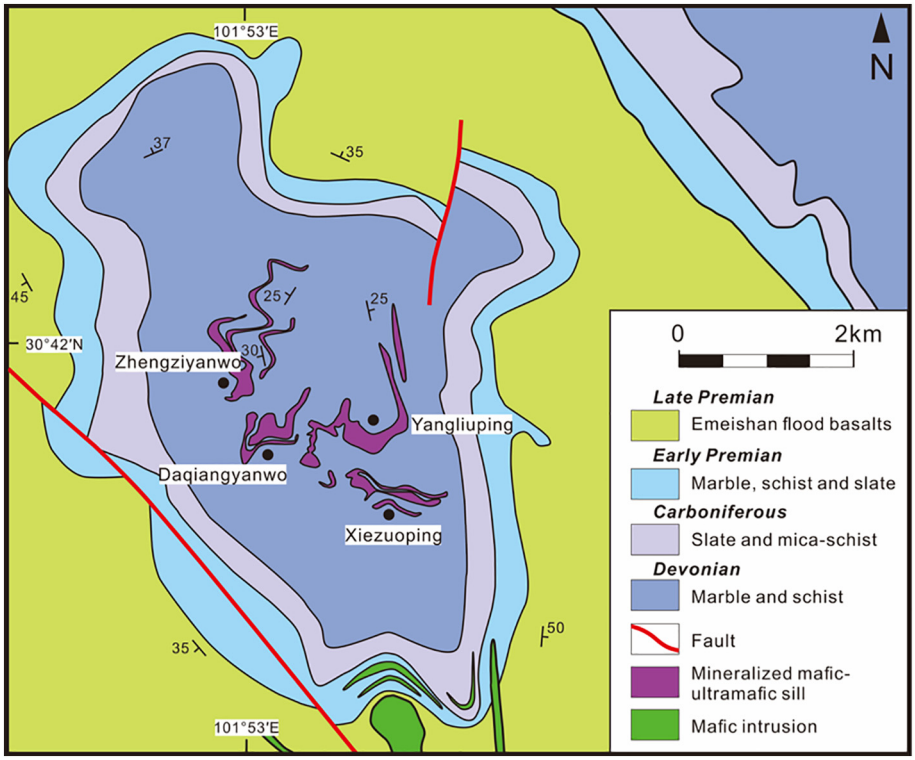

Fig. 1. Geological map of Yangliuping tectonic dome, southwestern China, showing the distribution of mafic-ultramafic sills within the dome. Modified after Song et al. (2004).

Ru, Pt, Pd, Te, Sn, Co, Ni) and sulfides (CdSe, FeAsS, Bi_2S_3, Sb_2S_3, PbS, ZnS, $CuFeS_2$) were used as standards. Detection limits are 440 ppm for Ir, 150 ppm for Ru, 270 ppm for Rh, 340 ppm for Pt, 150 ppm for Pd, 400 ppm for As, 680 ppm for Te, 160 ppm for Sn and 550 ppm for Cu in average.

LA-ICPMS was conducted on pyrrhotite, pentlandite, and chalcopyrite to determine the concentration of PGE present in those BMS (Table 4), chemical composition of subsurface PGE inclusion (Table 5) and these data were compared with the PGE whole rock assay data (Tables 1, 2). PGE concentrations were obtained by LA-ICPMS at CODES, University of Tasmania, using an Agilent 7700× quadrupole ICP-MS coupled to an ASI RESOLution-LR-S155 laser microprobe equipped with a Coherent Compex-Pro 193 nm ArF excimer laser. A laser beam of 29 μm was used with a pulse rate of 5 Hz and a fluence of 2.7 J/cm^2. Ablation was performed in a He atmosphere flowing at 0.35 L/min. The ablated aerosol was mixed with Ar (1.05 L/min) as a transport gas. The following isotopes measured were:^{34}S, ^{55}Mn, ^{57}Fe, ^{59}Co, ^{60}Ni, ^{65}Cu, ^{66}Zn, ^{75}As, ^{77}Se, ^{93}Nb, ^{99}Ru, ^{103}Rh, ^{106}Pd, ^{109}Ag, ^{111}Cd, ^{118}Sn, ^{121}Sb, ^{125}Te, ^{185}Re, ^{189}Os, ^{193}Ir, ^{195}Pt, ^{197}Au, ^{206}Pb, ^{209}Bi. At mean time, ^{87}Sr, ^{90}Zr, ^{92}Zr, ^{181}Ta were monitored to handle the potential interferences. Total acquisition time for each analysis was 90 s, comprising 30 s of gas background and 60 s of ablation signal. Signal quantification was carried following the standard methods (Longerich et al., 1996; Kosler, 2001). Po724-T (Sylvester et al., 2005), NiS_3 (Gilbert et al., 2013) and STDGL2b2 (Danyushevsky et al., 2011) reference materials were used for calibration. Oxidation yield ThO/Th < 0.1 was an important tuning parameter. And to confirm the contribution of oxygen, ^{29}Si and ^{45}Sc in quartz (in-house standard) were analyzed three times per hour during the whole test work.

Correlation for base metal-argide interferences is extremely important in LA-ICPMS PGE analysis, particularly for Ru, Rh and Pd (Cabri et al., 2017). The interferences could be ^{61}Ni^{40}Ar interferences on ^{101}Ru, ^{59}Co^{40}Ar on ^{99}Ru, ^{63}Cu^{40}Ar on ^{103}Rh, ^{65}Cu^{40}Ar on ^{105}Pd, and ^{66}Zn^{40}Ar on ^{106}Pd. The production of extent of base metal-argide were determined by ablating pure Co, Ni, Cu and Zn, and a correction factor was applied to the results to quantification the Ru, Rh and Pd. By recording the signal of ^{111}Cd, the isobaric interference of ^{106} Cd on ^{106}Pd were corrected.

To a certain extent, selective integration of signals could minimize contributions from interfering elements. Such as inclusions of sphalerite gives ^{66}Zn^{40}Ar and ^{106}Cd interferences on ^{106}Pd, ^{68}Zn^{40}Ar and ^{108}Cd on ^{108}Pd. Similarly, ^{87}Sr^{16}O, ^{90}Zr^{16}O, ^{92}Zr^{16}O, ^{181}Ta^{16}O interfere with ^{103}Rh, ^{106}Pd, ^{108}Pd and ^{197}Au respectively (Cabri et al., 2017). Thus, micro-inclusion (such as sphalerite inclusion) was avoided when selecting interval of the analyses without PGE inclusion (Fig. 5A, B, C; Table 4). As for the analyses with subsurface PGE inclusion (Table 5), the interval of PGE peaks was selected for integration (Fig. 5D, E F).

5. Analytic results

5.1. Whole rock PGE and semimetal element concentrations

As shown in Table 2 and Fig. 2, PGE tenors of the Yangliuping massive and disseminated ores are highly variable. The massive ores are relatively enriched in IPGE and Rh, containing 263 ppb Ir, 516 ppb Ru and 243 ppb Rh on average, and the disseminated ores contain 109 ppb Ir, 240 ppb Ru and 180 ppb Rh on average. In contrast, the massive ores are lower in Pt and Pd (1763 ppb and 2389 ppb in average, respectively) than the disseminated ores (2472 ppb and 6768 ppb in average, respectively) and appear to be depleted in Pt (Fig. 2). Thus, the massive ores have much lower Pd/Ir ratio (2 – 30) than the disseminated ores (7–1587).

Semimetal element concentrations in 100% sulfide are variable as listed in Table 2. Arsenic, Sb, Te and Bi concentrations are much lower than Se in both massive and disseminated ores. The disseminated ores are relatively rich in semimetal elements with 99.9 ppm As, 21.4 ppm Sb, 12.9 ppm Te, 6.2 ppm Bi, 136.7 ppm Se, while the massive ores contain 17.0 ppm As, 1.1 ppm Sb, 6.3 ppm Te, 1.9 ppm Bi and 123.3 ppm Se in average. Compared with the Jinchuan and Sudbury-Creighton deposits, the massive ores in the Yangliuping deposit are

Table 1
Whole-rock contents of S, metals and semimetal elements in the sulfide ores from the Yangliuping Ni–Cu-PGE deposit.

Sample	Ore type	S	Ni	Cu	Co	Os	Ir	Ru	Rh	Pt	Pd	As	Se	Sb	Te	Bi	Data source
		wt%	wt%	wt%	ppm	ppb	ppb	ppb	ppb	ppb	ppb	ppm	ppm	ppm	ppm	ppm	
SY16-2	MS	34.16	3.74	10.75	1180	183	126	195	147	2876	2038	16.6	120.0	1.3	7.9	1.5	This study
SY16-4	MS	31.20	4.49	0.16	1573	n.d.	109	434	131	2317	2043	17.1	108.0	0.7	5.1	1.9	This study
SY16-5	MS	34.40	4.88	0.22	1416	n.d.	213	447	166	1101	2583	35.7	82.0	0.7	4.0	0.8	This study
SY16-21	MS	33.92	4.39	5.10	1337	n.d.	211	440	153	3992	3141	7.7	126.0	1.8	5.8	2.4	This study
SY16-23	MS	32.64	5.34	0.47	1573	n.d.	–	322	151	1968	937	12.8	102.0	0.3	5.0	0.8	This study
Y01-44	MS	30.00	5.57	0.45	n.d.	n.d.	192	410	239	1797	1308	n.d.	n.d.	n.d.	n.d.	n.d.	Song et al., 2004
Y01-57	MS	34.30	5.53	0.04	n.d.	n.d.	483	674	332	380	1126	13.9	n.d.	n.d.	n.d.	n.d.	Song et al., 2004
Y02-2	MS	33.70	3.94	11.29	n.d.	n.d.	213	445	292	886	2236	12.3	n.d.	n.d.	n.d.	n.d.	Song et al., 2004
Y02-3	MS	33.70	4.54	10.00	n.d.	n.d.	162	519	225	1786	4867	10.1	n.d.	n.d.	n.d.	n.d.	Song et al., 2004
Z01-1	MS	26.05	5.02	0.13	31	n.d.	521	1033	339	150	1247	7.1	n.d.	0.7	n.d.	2.1	Song et al., 2004
ZD-22	MS	34.73	6.17	0.03	n.d.	n.d.	106	117	148	487	1997	n.d.	n.d.	n.d.	n.d.	n.d.	Song et al., 2004
ZD-25	MS	34.75	6.19	0.03	n.d.	n.d.	62	88	141	682	1493	n.d.	n.d.	n.d.	n.d.	n.d.	Song et al., 2004
SY16-10	DS	5.39	1.15	0.46	472	90	52	94	40	191	383	7.0	14.4	4.0	< 0.01	1.2	This study
SY16-12	DS	9.49	1.52	0.77	472	3	12	16	19	1509	1991	3.2	36.1	5.1	3.1	4.3	This study
SY16-39	DS	6.75	1.63	0.54	472	88	42	63	41	339	694	0.9	26.8	4.0	2.2	1.4	This study
SY16-47	DS	10.05	1.87	0.37	629	20	22	28	32	1030	774	1.3	40.3	2.7	3.7	2.1	This study
Z01-37	DS	10.20	1.84	0.38	532	n.d.	17	30	59	263	675	4.6	n.d.	0.4	n.d.	0.6	Song et al., 2004
Y01-38	DS	2.66	0.44	1.46	163	n.d.	1	3	20	288	1734	30.8	n.d.	2.0	n.d.	0.2	Song et al., 2004
Y01-55	DS	16.60	1.58	6.03	n.d.	n.d.	27	77	43	667	1378	5.8	n.d.	n.d.	n.d.	n.d.	Song et al., 2004
YD-2	DS	11.40	2.19	0.62	n.d.	n.d.	17	44	41	1135	3819	n.d.	n.d.	n.d.	n.d.	n.d.	Song et al., 2004
Z01-6	DS	2.50	0.39	0.14	161	n.d.	1	4	4	167	494	3.8	n.d.	1.0	n.d.	0.6	Song et al., 2004
Z01-32	DS	3.30	0.68	0.23	206	n.d.	3	15	10	280	410	1.9	n.d.	2.6	n.d.	0.8	Song et al., 2004
Z01-40	DS	6.86	1.04	0.92	326	n.d.	25	82	38	132	704	55.4	n.d.	15.0	n.d.	0.6	Song et al., 2004
Z01-43	DS	8.58	0.57	5.03	189	n.d.	7	16	46	146	2449	4.0	n.d.	1.3	n.d.	0.6	Song et al., 2004
Z02-1	DS	14.42	2.52	3.58	390	n.d.	60	94	87	855	1654	6.8	n.d.	0.7	n.d.	0.5	Song et al., 2004
Z02-2	DS	5.07	0.65	1.07	251	n.d.	32	99	39	272	665	47.2	n.d.	1.9	n.d.	0.3	Song et al., 2004

Note: MS = massive sulfide ore, DS = disseminated sulfide ore. “n.d.” = not detected.

slightly higher in As, Se and Te, but lower in Bi concentration (Fig. 3, Supplementary Table S1) (Chen et al., 2013, 2015; Dare et al., 2010b). Whereas the massive ores of the Noril'sk deposit are evidently barren in the semimetal elements (Fig. 3) (Zientek et al., 1994; Duran et al., 2017).

Table 2
Recalculated contents of S, metals and semimetal elements in the sulfide ores in bases of 100% sulfide.

Sample	Ore type	S	Ni	Cu	Co	Os	Ir	Ru	Rh	Pt	Pd	As	Se	Sb	Te	Bi	Data source
		wt%	wt%	wt%	ppm	ppb	ppb	ppb	ppb	ppb	ppb	ppm	ppm	ppm	ppm	ppm	
SY16-2	MS	37.23	4.08	11.72	1286	199	137	213	160	3135	2221	18.1	131	1.37	8.58	1.61	This study
SY16-4	MS	38.51	5.54	0.20	1942	n.d.	134	536	161	2860	2522	21.1	133	0.85	6.23	2.33	This study
SY16-5	MS	38.52	5.46	0.25	1585	n.d.	238	500	186	1233	2893	40.0	92	0.78	4.46	0.93	This study
SY16-21	MS	37.89	4.91	5.70	1493	n.d.	235	492	170	4458	3509	8.6	141	2.03	6.49	2.64	This study
SY16-23	MS	38.33	6.27	0.55	1847	n.d.	–	378	177	2311	1100	15.0	120	0.33	5.81	0.96	This study
Y01-44	MS	38.17	7.09	0.57	n.d.	n.d.	244	521	304	2287	1664	n.d.	n.d.	n.d.	n.d.	n.d.	Song et al., 2004
Y01-57	MS	38.41	6.19	0.04	n.d.	n.d.	541	755	372	426	1261	15.6	n.d.	n.d.	n.d.	n.d.	Song et al., 2004
Y02-2	MS	37.09	4.34	12.42	n.d.	n.d.	234	490	321	975	2461	13.5	n.d.	n.d.	n.d.	n.d.	Song et al., 2004
Y02-3	MS	37.15	5.01	11.02	n.d.	n.d.	179	572	248	1969	5366	11.1	n.d.	n.d.	n.d.	n.d.	Song et al., 2004
Z01-1	MS	38.17	7.36	0.19	45	n.d.	764	1514	496	220	1828	10.3	n.d.	0.97	n.d.	3.02	Song et al., 2004
ZD-22	MS	38.30	6.80	0.03	n.d.	n.d.	117	129	163	537	2203	n.d.	n.d.	n.d.	n.d.	n.d.	Song et al., 2004
ZD-25	MS	38.30	6.82	0.03	n.d.	n.d.	68	97	155	752	1645	n.d.	n.d.	n.d.	n.d.	n.d.	Song et al., 2004
SY16-10	DS	37.64	8.04	3.21	3298	627	363	655	279	1335	2676	48.9	101	27.60	n.d.	8.45	This study
SY16-12	DS	38.02	6.09	3.08	1890	13	46	63	76	6045	7975	12.9	145	20.59	12.22	17.14	This study
SY16-39	DS	37.48	9.08	2.97	2621	488	232	348	227	1883	3854	4.8	149	22.38	12.27	7.72	This study
SY16-47	DS	38.06	7.08	1.40	2382	77	84	106	121	3900	2931	4.9	153	10.07	14.16	8.10	This study
Z01-37	DS	38.10	6.88	1.40	1989	n.d.	64	114	219	981	2521	17.3	n.d.	1.61	n.d.	2.15	Song et al., 2004
Y01-38	DS	35.82	5.86	19.69	2201	n.d.	15	39	274	3880	23,348	415.1	n.d.	27.00	n.d.	3.33	Song et al., 2004
Y01-55	DS	37.10	3.53	13.48	n.d.	n.d.	60	171	96	1491	3079	13.0	n.d.	n.d.	n.d.	n.d.	Song et al., 2004
YD-2	DS	37.93	7.29	2.06	n.d.	n.d.	55	146	137	3777	12,708	n.d.	n.d.	n.d.	n.d.	n.d.	Song et al., 2004
Z01-6	DS	38.17	5.93	2.16	2466	n.d.	20	54	59	2547	7549	57.6	n.d.	15.12	n.d.	9.22	Song et al., 2004
Z01-32	DS	37.77	7.81	2.59	2357	n.d.	32	167	115	3207	4695	21.6	n.d.	29.30	n.d.	9.33	Song et al., 2004
Z01-40	DS	37.82	5.73	5.06	1797	n.d.	136	453	211	729	3881	305.2	n.d.	82.44	n.d.	3.06	Song et al., 2004
Z01-43	DS	36.26	2.40	21.24	799	n.d.	30	68	193	616	10,351	16.7	n.d.	5.42	n.d.	2.63	Song et al., 2004
Z02-1	DS	37.12	6.48	9.23	1004	n.d.	154	243	223	2201	4258	17.5	n.d.	1.90	n.d.	1.24	Song et al., 2004
Z02-2	DS	37.59	4.84	7.97	1861	n.d.	237	734	287	2014	4927	349.8	n.d.	13.84	n.d.	2.03	Song et al., 2004

Note: MS = massive sulfide ore, DS = disseminated sulfide ore. “n.d.” = not detected.
Using $C_{(100\%\ Sul)} = C_{wr}*100/(2.527*S + 0.3408*Cu + 0.4715*Ni)$ (Barnes and Lightfoot, 2005) to recalculate, where C_{wr} = concentration of the element in the whole rock. S, Ni and Cu = concentration of these elements in the whole rock (wt%).

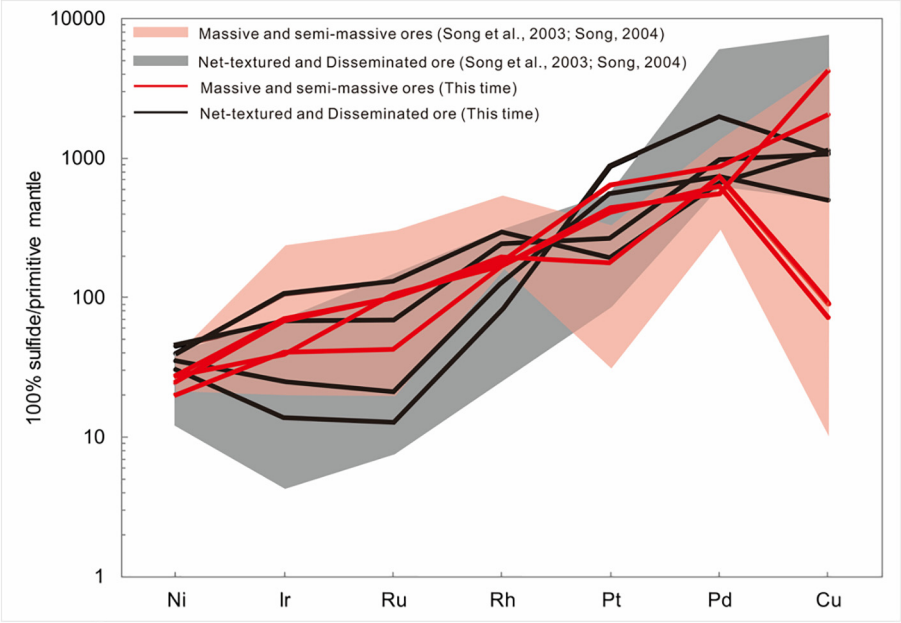

Fig. 2. Primitive mantle-normalized whole rock PGE patterns for massive and disseminated ores from Yangliuping deposit (normalized to 100% sulfide). Primitive mantle values are from Barnes and Maier (1999).

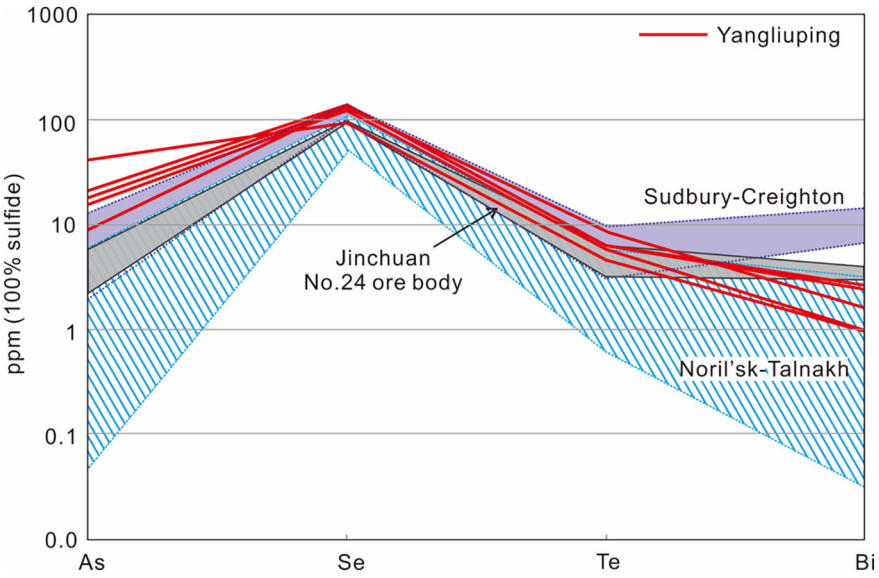

Fig. 3. Semimetal elements patterns on 100% sulfide of massive ores from Yangliuping (this study), Jinchuan-No.24 ore body (Chen et al., 2013; Chen et al., 2015), Sudbury-Creighton (Dare et al., 2010a) and Noril'sk-Talnakh (Zientek et al., 1994; Duran et al., 2017). Some unpublished data from the Jinchuan and the Noril'sk deposits were also include.

5.2. PGE and semimetals in CGSS and BMS

In this study, 90 CGSS grains have been identified (Table 7). Most of them are found in the massive ores, in which the CGSS are larger (up to 30 μm in diameter) than in the disseminated ores (1–3 μm in diameter). The CGSS are euhedral and subhedral and predominantly enclosed in pyrrhotite and occasionally within pentlandite and chalcopyrite (Fig. 4). The CGSS crystals show a clear core-rim texture (Fig. 4D, G, I) or oscillatory zonation (Fig. 4C, H) in backscattered electron images. The cores of the CGSS are commonly richer in PGE and poorer in Co than the rims (Table 3). Nanometer-size PGE-arsenides or sulfarsenides, 100–500 nm in diameter, are quite common in the core or mantle of the CGSS, while altaite or galena may occur at the boundaries of the CGSS crystals (Fig. 4, Table 6).

LA-ICPMS measurements indicate that pyrrhotite, pentlandite and chalcopyrite contain much less PGE than the CGSS in the Yangliuping deposit (Table 4). Iridium, Rh and Pt concentrations of the pyrrhotite, pentlandite and chalcopyrite are commonly undetectable. Pentlandite is most enriched in Pd (862–5898 ppb) and pyrrhotite is slightly more enriched in Os (73–189 ppb), while chalcopyrite is relatively barren in all PGE. Pentlandite in the massive ore is higher in Pd concentrations (1422 to 5898 ppb) than that in the disseminated ores (Pd = 862 ppb) (Table 4). Both pyrrhotite and pentlandite are rich in Ru (136–448 and 226–441 ppb, respectively) (Table 4). Spectra of most LA-ICPMS measuring points do not display PGE peaks thus indicating that PGE are hosted in most areas of the BMS grains as solid solution (Fig. 5A, B, C).

On the other hand, LA-ICPMS time-resolved spectra of a few points on pyrrhotite, pentlandite and chalcopyrite show real peaks of Ir, Rh and Pt as well as Os and Ru occasionally (Fig. 5D, E, F), which indicates the presence of tiny subsurface PGE-rich inclusions in the BMS (Table 5) (Ballhaus and Sylvester, 2000; Godel et al., 2007). Consistently, LA-ICPMS maps display an overlap of the Os, Ir, Rh, Pt and As enrichment points in both pyrrhotite and pentlandite (Fig. 6). Calculations according to the accounts of the narrow intervals showing peaks

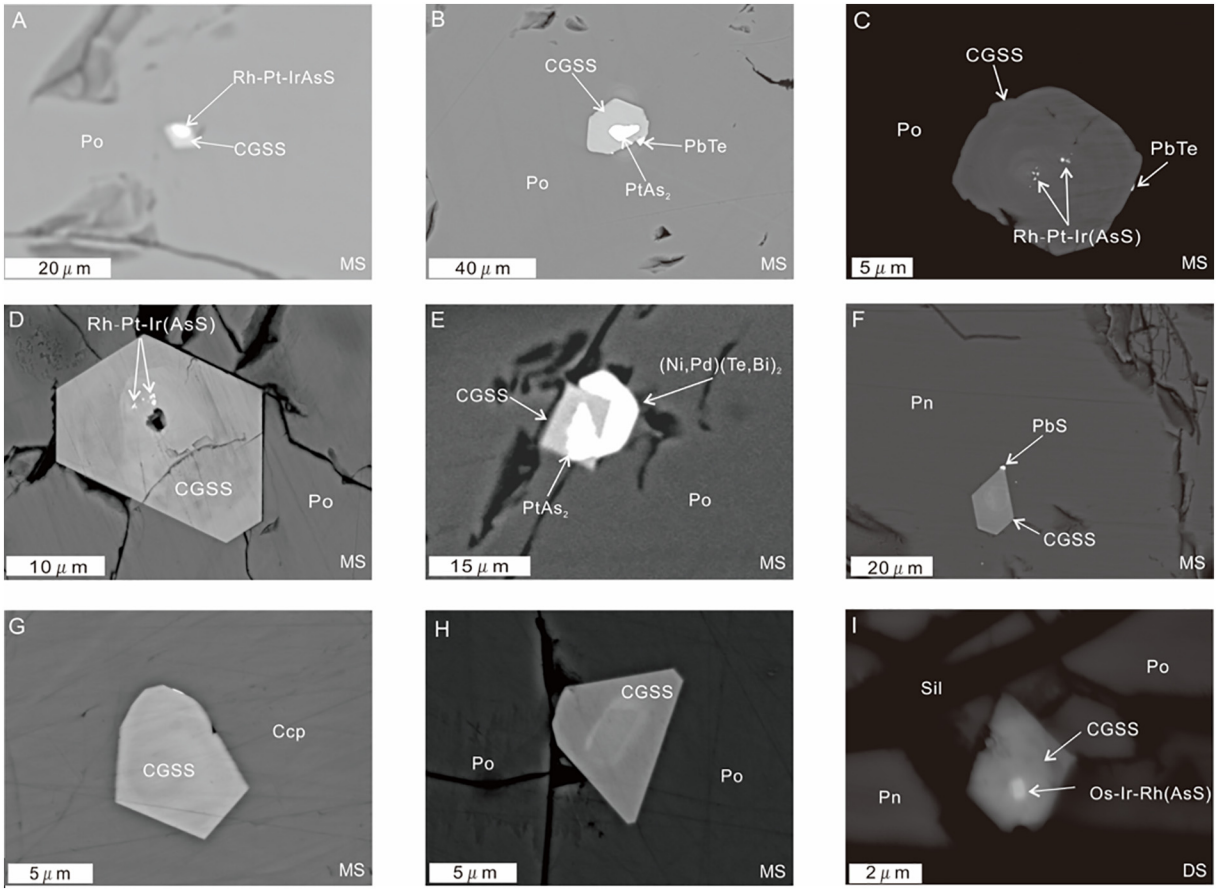

Fig. 4. Backscattered electron (BSE) images of cobaltite-gersdorffite solid solution (CGSS) with different characters. CGSS were mainly found in massive ores (A-H), only a few of CGSS with much small diameter were found in disseminated ores (I). A. Euhedral CGSS with a Pt-Rh-IrAsS core in pyrrhotite. B. Euhedral CGSS containing a $PtAs_2$ and a small particle of altaite at rim hosted in pyrrhotite. C and D. CGSS with oscillatory zonation contain several nanometer-size PGE-arsenides and sulfarsenides. Note that the nanometer-size PGE-arsenides and sulfarsenides are not always occur in the core of the CGSS. E. CGSS contain anhedral sperrylite core and surrounded by a partial rim of subhedral Pd melonite. F. Euhedral CGSS in spatial association with galena. G and H. Subhedral CGSS with a brighter core enclosed in chalcopyrite and pyrrhotite. I. CGSS with nanometric Os-Ir-Rh(AsS) core and located at boundary of pentlandite and pyrrhotite. Abbreviations: CGSS = cobaltite-gersdorffite solid solution, $PtAs_2$ = sperrylite, Ccp = chalcopyrite, Po = pyrrhotite, Pn = pentlandite. PbTe = altaite, $(Ni,Pd)(Te,Bi)_2$ = Pd melonite, PbS = galena.

Table 3
Compositions (in wt%) of CGSS in the massive ores from the Yangliuping deposit analyzed by EPMA.

Sample	Grain	Position	S	Fe	Co	Ni	As	Os	Ir	Ru	Rh	Pt	Pd	Cu	Total
SY16-2	1		19.5	8.98	14.3	15.5	40.2	–	0.201	0.241	0.068	0.218	1.02	–	100.3
	2	Core	18.0	7.98	10.8	16.6	43.8	0.637	0.152	0.272	0.885	0.294	1.28	–	100.7
		Rim	17.6	7.11	13.8	22.3	37.4	0.580	0.146	0.279	0.034	0.215	0.718	–	100.1
	3		18.5	8.07	13.5	14.9	42.4	0.630	0.275	0.227	0.025	0.289	0.860	0.297	100.0
	4	Core	17.1	7.45	10.6	15.9	43.1	0.957	0.092	0.263	1.95	0.557	1.74	1.26	101.0
		Rim	17.9	7.77	13.2	14.0	44.1	0.926	0.055	0.259	0.041	0.421	0.958	1.54	101.2
	5	Core	16.9	7.03	12.6	12.8	42.3	2.66	1.37	0.267	1.12	0.564	1.50	1.40	100.5
		Rim	17.9	7.82	12.9	14.2	43.3	1.04	0.203	0.268	0.065	0.421	1.00	1.39	100.5
	6	Core	17.5	8.18	10.0	15.0	43.0	0.726	0.396	0.282	2.63	0.714	2.40	–	100.8
		Rim	18.4	8.89	13.6	14.1	44.1	0.111	0.060	0.239	0.011	0.248	0.963	–	100.7
	7		18.6	8.50	14.7	12.7	44.2	–	0.115	0.228	0.061	0.183	0.819	–	100.0
	8		17.8	8.30	11.1	15.8	44.5	0.437	0.138	0.219	0.632	0.200	1.18	–	100.2
	9	Core	18.1	7.65	10.8	15.7	43.7	0.241	0.142	0.138	1.39	0.503	1.57	–	99.9
		Mantle	18.6	7.71	14.6	13.3	44.2	0.132	–	0.113	0.024	0.419	1.00	–	100.1
		Rim	19.0	7.15	18.2	11.1	43.6	0.200	0.092	0.078	0.051	0.442	0.557	–	100.4
SY16-4	1		17.9	8.28	13.6	15.5	42.9	0.381	0.065	0.275	0.073	–	0.829	–	99.7
	2	Core	17.0	7.45	10.2	17.7	42.4	0.642	0.262	0.345	2.29	0.006	1.97	–	100.2
		Rim	17.4	8.11	13.3	14.8	43.6	0.260	0.055	0.320	0.042	0.447	1.11	–	99.4
SY16-23	1	Core	16.8	7.90	10.3	15.1	43.3	0.739	0.465	0.339	2.96	0.632	2.46	–	101.0
		Rim	17.3	7.85	11.3	12.9	42.8	2.11	0.467	0.302	1.36	0.509	1.30	1.56	99.7
	2		18.0	8.08	16.8	11.5	42.9	0.927	0.346	0.333	0.125	0.831	0.419	–	100.3
	3		20.4	12.8	17.9	8.73	39.7	0.142	0.082	0.324	0.035	0.440	0.175	–	100.8

M = massive ore. "–" blew the detection limit.
Detection limit (ppm): S > 310, Fe > 270, Co > 310, Ni > 280, As > 410, Os > 1590, Ir > 441, Ru > 150, Rh > 270, Pt > 340, Pd > 150, Cu > 550.

Table 4
LA-ICP-MS analysis results for pyrrhotite, pentlandite, and chalcopyrite without PGE inclusions from the Yangliuping deposit.

Sample	Ore	Point	^{61}Ni	^{65}Cu	^{185}Re	^{192}Os	^{193}Ir	^{101}Ru	^{103}Rh	^{195}Pt	^{105}Pd	^{197}Au	^{107}Ag	^{59}Co	^{75}As	^{77}Se	^{118}Sn	^{121}Sb	^{125}Te	^{209}Bi	inclusion
			wt%	wt%	ppb	ppb	ppb	ppb	ppb	ppb	ppb	ppb	ppm	ppm	ppm	ppm	ppm	ppm	ppm	ppm	
Chalcopyrite																					
SY16-2	MS	1	0.03	36.5	< 10	< 8	< 14	39	< 3	11	372	< 17	100	2.49	< 0.52	126	2.65	0.10	1.44	0.12	No
		2	0.01	36.8	< 10	< 8	< 14	37	< 3	< 8	398	< 17	19.5	2.43	< 0.46	141	3.04	0.04	2.47	0.08	No
SY16-4	MS	3	0.00	36.3	< 10	< 8	< 14	29	27	< 8	381	< 17	3.32	0.637	< 0.70	116	28.8	0.07	1.71	0.10	No
Pentlandite																					
SY16-4	MS	1	33.8	0.0001	15	81	17	380	8	< 8	1834	< 17	1.02	11,986	< 0.95	91.2	< 0.05	0.03	0.14	0.03	No
		2	33.6	< 0.0001	11	49	< 14	310	< 3	< 8	1516	< 17	1.08	12,563	< 1.08	92.2	< 0.05	0.03	0.39	0.07	No
		3	33.9	0.0002	13	84	< 14	346	4	< 8	4918	< 17	0.95	12,090	< 0.36	80.1	0.02	0.02	0.84	0.00	No
		4	34.2	0.0001	< 10	55	< 14	322	< 3	< 8	2419	< 17	0.72	13,365	< 0.48	80.8	0.04	0.04	0.18	0.01	No
		5	34.1	0.0001	17	26	< 14	226	< 3	< 8	1999	< 17	0.57	13,926	< 0.46	82.7	< 0.02	0.01	0.29	0.01	No
		6	33.5	0.0001	12	42	< 14	243	4	< 8	2233	< 17	0.48	13,454	< 0.42	78.8	< 0.02	0.01	0.25	0.02	No
		7	35.8	< 0.0001	11	32	< 14	320	< 3	< 8	2070	< 17	0.55	13,823	< 0.49	82.4	0.04	0.02	0.34	0.00	NO
		8	35.1	0.0001	< 10	81	< 14	284	< 3	< 8	1962	< 17	0.23	13,835	< 0.43	79.4	< 0.02	0.02	0.15	0.01	No
		9	34.2	< 0.0001	< 10	47	< 14	255	< 3	< 8	1613	< 17	0.77	13,748	3.74	87.6	0.08	0.45	0.51	0.38	No
		10	35.1	< 0.0001	11	68	< 14	340	27	< 8	1550	< 17	0.52	13,784	< 0.70	91.6	0.18	0.03	< 0.11	0.03	No
		11	35.1	< 0.0001	< 10	79	< 14	412	6	< 8	1422	< 17	0.43	13,324	< 0.45	79.8	0.03	0.02	0.17	0.05	No
		12	33.9	0.0001	11	79	< 14	344	5	< 8	5596	< 17	0.45	15,147	< 0.47	82.4	0.05	0.04	2.17	0.02	No
		13	35.0	0.0001	14	72	< 14	287	< 3	< 8	5470	< 17	0.53	14,786	< 0.44	78.9	0.03	0.05	0.14	0.00	No
		14	36.1	0.0001	< 10	46	< 14	441	< 3	< 8	5898	< 17	0.50	15,967	< 0.42	80.1	< 0.02	0.05	0.28	0.10	No
SY16-47	DS	15	39.4	0.0001	< 10	105	< 14	434	60	< 8	862	< 17	3.17	11,936	1.70	119	< 0.04	6.50	10.66	5.26	No
Pyrrhotite																					
SY16-2	MS	1	1.65	0.0001	12	96	< 14	172	< 3	< 8	< 11	< 17	0.12	231	< 0.71	161	< 0.04	< 0.01	0.46	0.07	No
		2	1.57	0.0002	15	98	< 14	173	9	< 8	< 11	< 17	0.05	230	< 0.60	161	0.06	0.02	0.16	0.04	No
		3	1.59	0.0001	< 10	104	< 14	136	12	< 8	< 11	< 17	0.05	220	< 0.69	162	< 0.04	0.01	0.34	0.02	No
SY16-4	MS	4	0.98	< 0.0001	22	112	< 14	248	6	< 8	< 11	< 17	0.17	203	< 0.80	146	< 0.05	< 0.01	< 0.09	0.08	No
Sample	Ore	Point	^{61}Ni	^{65}Cu	^{185}Re	^{192}Os	^{193}Ir	^{101}Ru	^{103}Rh	^{195}Pt	^{105}Pd	^{197}Au	^{107}Ag	^{59}Co	^{75}As	^{77}Se	^{118}Sn	^{121}Sb	^{125}Te	^{209}Bi	Inclusion
			wt%	wt%	ppb	ppb	ppb	ppb	ppb	ppb	ppb	ppb	ppm	ppm	ppm	ppm	ppm	ppm	ppm	ppm	
Pyrrhotite																					
SY16-4	MS	5	0.92	< 0.0001	12	104	< 14	257	8	< 8	< 11	< 17	0.37	204	< 0.78	145	< 0.03	< 0.01	0.32	0.11	No
		6	0.95	< 0.0001	11	114	< 14	233	6	9	< 11	< 17	0.23	242	< 0.77	133	< 0.03	< 0.01	0.28	0.16	No
		7	1.43	< 0.0001	20	123	< 14	215	< 3	< 8	< 11	< 17	0.13	169	< 0.78	148	< 0.03	< 0.01	0.29	0.06	No
SY16-39	DS	8	3.35	< 0.0001	< 10	101	< 14	223	< 3	< 8	< 11	< 17	0.69	535	< 0.95	147	0.35	5.54	1.39	0.94	No
		9	3.56	0.0001	< 10	73	< 14	448	10	< 8	25	< 17	3.09	555	1.15	144	0.25	6.36	1.25	13.7	No
		10	3.36	< 0.0001	16	189	< 14	383	54	< 8	< 11	< 17	0.32	558	< 0.82	156	< 0.03	0.50	1.62	0.98	No

Note: MS = massive sulfide ore, DS = disseminated sulfide ore, " < 14" = lower than detection limit, in this case of Ir, the detection limit is 14 ppb. The detection limit of PGE and Cu is average detection limit.

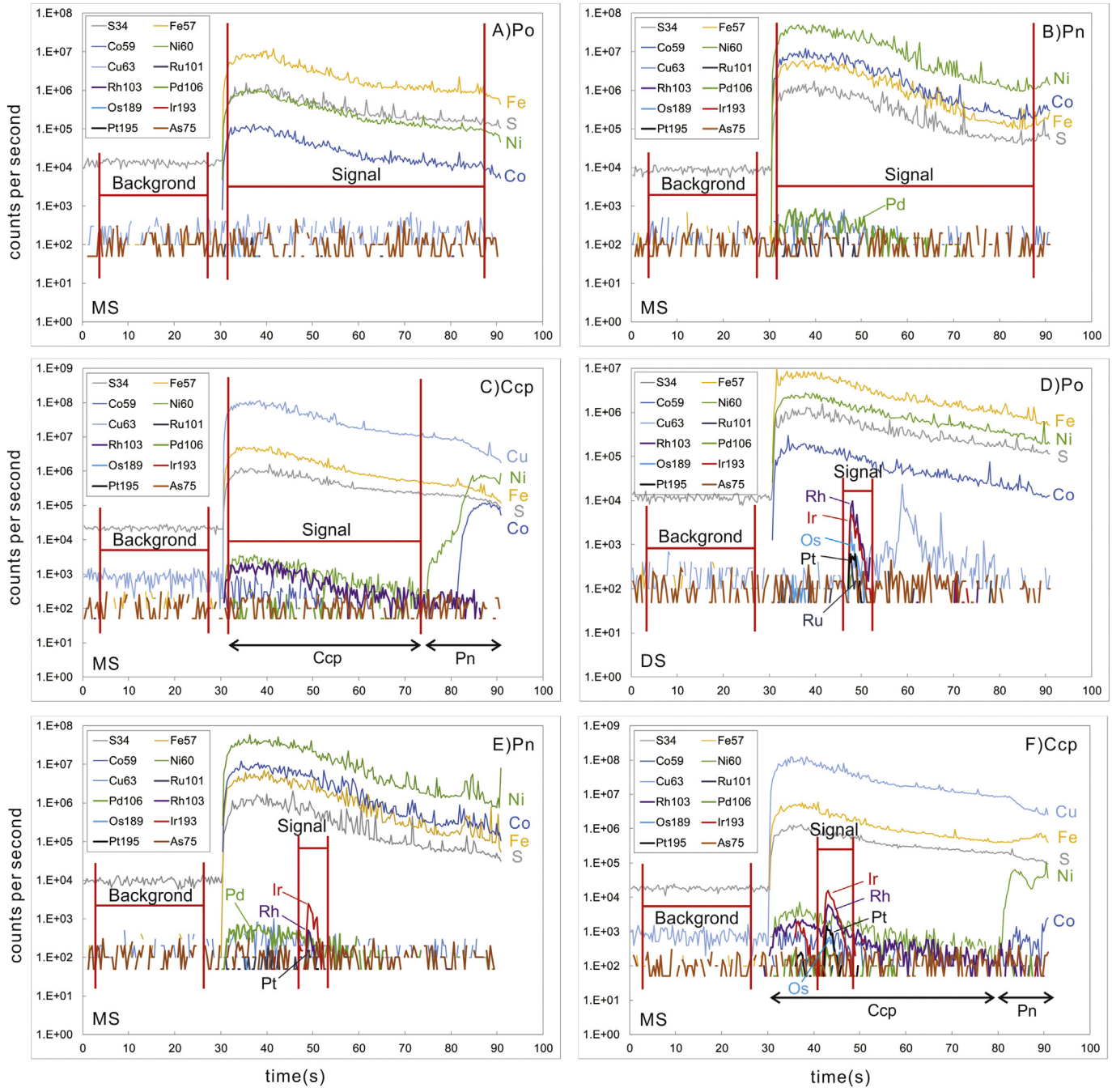

Fig. 5. Typical time-resolved spectra of LA-ICPMS. A–C. Spectrum from pyrrhotite (A), pentlandite (B) and chalcopyrite (C) show flat signal, no PGE inclusion were observed. D-F. Spectrum contain PGE inclusion. D. Pyrrhotite with Os-Ir-Ru-Rh-Pt inclusion. E. Pentlandite with Ir-Rh-Pt inclusion. F. Chalcopyrite with Os-Ir-Rh-Pt inclusion. The speculated width of the PGE inclusions was about 0.8 μm, 0.8 μm and 1.9 μm in D, E and F, respectively.

(Figs. 5D, E, F) of PGE indicate that the tiny PGE-rich inclusions are evidently high in Ir, Rh and Pt and highly variable in Os and Ru (Table 5). Ir and Pt concentrations are always lower than the detection limits for the measurement points without PGE-rich inclusions (Figs. 5A, B, C, Table 4). Palladium concentration is high in pentlandite and decreases gradually towards the phase boundary with pyrrhotite (Fig. 6H). In contrast, Bi is concentrated at the interface between the pyrrhotite and pentlandite or in fractures in the grains (Fig. 6L). Cobalt is strongly enriched in pentlandite (average 13,582 ppm) relative to pyrrhotite (average 315 ppm) and chalcopyrite (1–2 ppm) (Table 4).

As listed in Table 4, Se is the most abundant semimetal element in the BMS (133–162 ppm in pyrrhotite, 79–119 ppm in pentlandite and 116–141 pm in chalcopyrite) and As is usually lower than the detection limit of LA-ICPMS (0.63 ppm in average). The concentration of Sn, Sb, Te and Bi in the BMS is mostly below 1 ppm and only occasionally up to 29 ppm (Table 4).

5.3. Micrometer and nanometer-size PGM in BMS and CGSS

As shown in Fig. 4, micrometer and nanometer-size individual Ir-Rh-Pt sulfarsenides and clusters appear in the core and mantle of the CGSS. Micrometer-size euhedral to subhedral sperrylite crystals are enclosed in the CGSS (Fig. 4B) as well as BMS (Fig. 7A, B) and occasionally enclosed by other PGM, such as testibiopalladite (Fig. 7C). Testibiopalladite grains, up to 40 μm in length, are enclosed in pyrrhotite and pentlandite or located at the boundaries between BMS

Table 5
LA-ICP-MS analysis results for pyrrhotite, pentlandite, and chalcopyrite containing subsurface PGE-rich inclusions from the Yangliuping deposit.

Sample	Ore	Point	^{61}Ni	^{65}Cu	^{185}Re	^{192}Os	^{193}Ir	^{101}Ru	^{103}Rh	^{195}Pt	^{105}Pd	^{197}Au	^{107}Ag	^{59}Co	^{75}As	^{77}Se	^{118}Sn	^{121}Sb	^{125}Te	^{209}Bi	Inclusion[a]	Width (μm)
			wt%	wt%	ppb	ppb	ppb	ppb	ppb	ppb	ppb	ppb	ppm	ppm	ppm	ppm	ppm	ppm	ppm	ppm		
Chalcopyrite																						
SY16-4	MS	1	0.00	36.1	14	550	2981	134	779	665	218	< 17	3.75	1.36	0.66	126	28.3	0.05	2.64	0.08	Os-Ir-Ru-Rh-Pt-AsS	1.9
		2	0.00	36.1	< 10	27	237	46	< 3	36	239	< 17	3.39	0.864	< 0.65	152	20.2	0.10	2.80	0.11	Os-Ir-Pt-AsS	1.5
Pentlandite																						
SY16-4	MS	1	34.3	0.0001	16	91	274	301	55	50	1833	< 17	0.4	14364	< 0.74	85.5	0.05	< 0.01	< 0.13	< 0.02	Os-Ir-Rh-Pt-AsS	0.8
SY16-47	DS	2	31.3	< 0.0001	< 10	218	214	598	109	31	45	< 17	3.53	8855	11.54	170	0.29	12.9	31.9	1.83	Os-Ir-Ru-Rh-Pt-AsS	1.1
Pyrrhotite																						
SY16-4	MS	1	1.23	< 0.0001	15	179	70	265	3	25	< 11	< 17	0.11	268	< 0.76	146	< 0.04	< 0.01	0.19	0.07	Ir-Rh-Pt-AsS	0.8
		2	1.19	0.0001	< 10	124	121	303	36	43	< 11	< 17	0.12	285	0.79	142	< 0.04	0.03	0.42	0.08	Ir-Rh-Pt-AsS	0.4
		3	1.09	< 0.0001	33	202	343	315	61	34	< 11	< 17	0.12	298	< 0.86	140	< 0.04	< 0.00	0.64	0.10	Ir-Rh-AsS	0.8
SY16-47	DS	4	2.81	0.0007	< 10	954	801	659	1210	286	88	< 17	1.04	382	< 0.98	150	0.07	1.51	1.53	11.0	Os-Ir-Ru-Rh-Pt-AsS	0.4

Note: MS = massive sulfide ore, DS = disseminated sulfide ore, " < 14" = lower than detection limit, in this case of Ir, the detection limit is 14 ppb.
[a] No As and S peaks was observed. LA-ICPMS mapping shows that As and PGE rich spots overlap each other very well (Fig. 6), thus those PGE inclusion probably are PGE-sulfarsenides. The duration time and the minimum width of PGE inclusion was speculated following the mothed of Godel et al. (2007). The empirical ablation rate of 1 μm/s was used for width calculation.

grains (Figs. 7C, D).

54 nanometer-size PGM were observed in pyrrhotite, pentlandite, and chalcopyrite in the massive and disseminated ores. Using high-resolution SEM (Table 6, Fig. 8), they are euhedral with grain size varying from < 100 to 500 nm, up to 800 nm in diameter (Fig. 8A-F). SEM-EDX measurements indicated that most of the nanometer-size PGM are sulfarsenides of Os-Ir-Ru-Rh-Pt after subtracting matrix elements (Fe, Ni, Cu and S) from the analyses (Zelenski et al., 2017). The detection limit for PGE using EDX is approximately 0.07 atom% (Wirth et al., 2013). This means that the same solid solution mineral may be identified as distinct species of sulfarsenide depending on whether PGE concentrations are higher than detection limit of EDX. Extensive solid solution among irarsite (IrAsS)-hollingworthite (RhAsS)-platarsite (PtAsS) has already been reported by previous studies (Tarkian and Prichard, 1987; Cabri, 2002). Thus, the nanometer-size sulfarsenides of Os-Ir-Ru-Rh-Pt listed in Table 6 in fact should belong to the (Ir, Rh, Pt)AsS solid solution with variable amount of Ru and Os. In backscattered electron images, the nanometer-size PGE-sulfarsenides may have brighter core and darker rims (Fig. 8B, D, E). SEM-EDX analysis indicates that the rims of the PGE-sulfarsenides (marked as ① in Fig. 8D, E) are richer in Ni and Co than the cores (marked as ②). The peaks of Ir, Rh, Pt and Os in pyrrhotite, pentlandite, and chalcopyrite revealed by time resolved spectra and enrichment points of these elements displayed by LA-ICPMS mapping (Figs. 4 and 5) match element assemblage of the nanometer-size PGE-sulfarsenides very well (Fig. 8).

6. Discussion

The above observations indicate that the mode of occurrence of PGE in the Yangliuping deposit have some distinct features. Comparing with the Jinchuan, Sudbury and Noril'sk deposits, the Yangliuping ores are characterized by relatively lower percentages of PGE hosted by BMS as solid solution in the BMS. Many nanometer- and micrometer-size PGE-arsenides and sulfarsenides are located in base-metals sulfides and CGSS. The euhedral CGSS crystals commonly have cores very enriched in PGE and rims rich in Co. On the other hand, the sulfide ores at Yangliuping are enriched in As compared with those at Noril'sk and Jinchuan. No magmatic PGE-selenides are known, this is consistent with the experimental evidence that PGE-Se are low temperature phases (Helmy and Fonseca, 2017).

Helmy and Bragagni (2017) found experimentally that Ir and Rh tend to form sulfarsenides and Pt and Pd tend to form semimetal phases like sperrylite or telluride (O'Driscoll and González-Jiménez, 2016). It has been proposed that the formation of arsenides and sulfarsenides is because of the strong affinity between PGE and semimetal elements, especially arsenic, which is commonly the most important semimetal element in sulfide melts at magmatic temperatures (Canali et al., 2017; Helmy and Bragagni, 2017). This is supported by the occurrences of Ir, Rh and Pt sulfarsenides and absence of any PGE-selenides in the Yangliuping deposit.

Both PGE and semimetals are trace elements and far from chemical saturation in the natural sulfide liquids (Helmy et al., 2013a; Bai et al., 2017). Thus, the PGM in the magmatic sulfide deposits are considered to have been formed at the last stage of sulfide liquid crystallization when semimetal contents reach saturation, or at the margins of crystallizing MSS or ISS where semimetals may reach saturation due to slow diffusion (Power et al., 2004; Barnes et al., 2006; Hutchinson and McDonald, 2008). Alternatively, nanometer-size PGE-arsenides and sulfarsenides associations can form directly from highly undersaturated sulfide melts (Helmy et al., 2013b). On the other hand, IPGE are compatible with MSS and Pt and Pd are incompatible (Ballhaus et al., 2001; Barnes et al., 2001; Mungall et al., 2005). This means that IPGE can be contained in the crystal lattice of MSS as solid solution. The PGM enclosed in pyrrhotite and pentlandite could be interpreted as the results of sub-solidus exsolution during cooling (e.g., Makovicky et al., 1986; Makovicky, 2002; Godel et al., 2007; Barnes et al., 2008; Godel

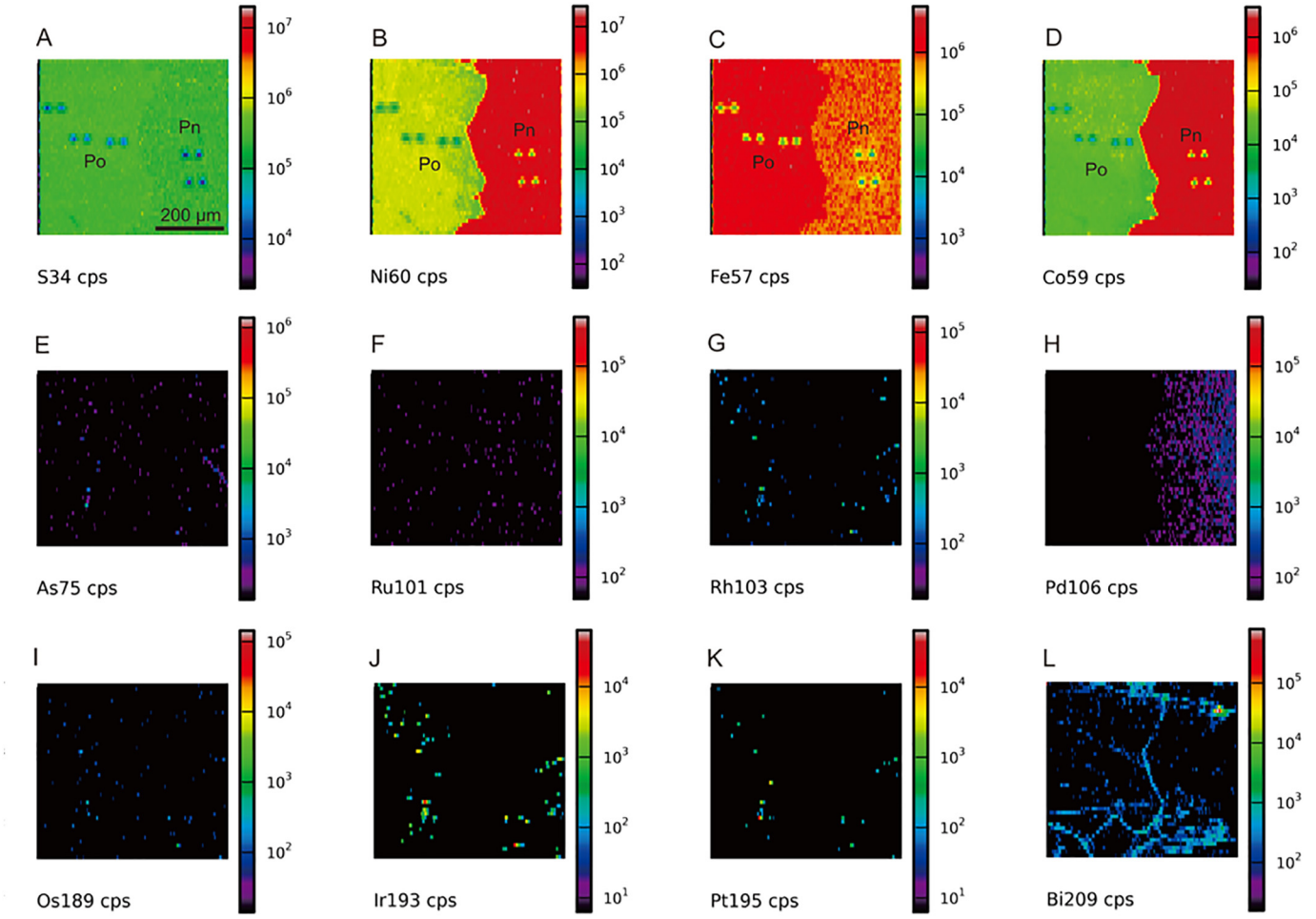

Fig. 6. LA-ICPMS mapping of S, Ni, Fe, Co, As, Ru, Rh, Pd, Os, Ir, Pt, Bi in pyrrhotite and pentlandite from massive ore. The rounded hole in A, B, C, and D is the position of spot analysis. Note that heterogeneous distribution of PGE and Bi in pyrrhotite and pentlandite. Thus, the PGE rich spots observed in E, F, G, I, J and K should be PGE-rich particles and Rh, Os, Ir and Pt are correlated with each other well.

and Barnes, 2008; Hutchinson and McDonald, 2008). Thus, the residual sulfide melt is gradually depleted in IPGE, and the chalcopyrite exsolved from ISS should not be expected to contain the same PGM as pyrrhotite and pentlandite.

Recent studies using LA-ICPMS demonstrated that there is a large variation on the concentration of PGE contained in BMS from different deposits (Fig. 9). Barnes et al. (2008) proposed that PGE (except for Pt) prefer to enter the BMS in solid solution during relatively rapid cooling, like the sulfide droplets from a sub-volcanic sill in the Noril'sk deposit. Whereas, in large and slowly cooling intrusions, it was expected that PGE could have exsolved from BMS to form PGM. In contrast, Hutchinson and McDonald (2008) proposed that semimetals in sulfide melt could prevent PGE enter MSS as solid solution and are conducive for PGM to crystallize early at high temperature in the Platreef of the Bushveld Complex. The Yangliuping sulfide ores are markedly enriched in As relative to the Noril'sk sulfide ores (Fig. 3) and abundant micrometer- and nanometer-size PGM have been observed as described above (Figs. 4, 5, 7, 8). These phenomena provide a good opportunity for better understanding the effects of semimetals on the behaviour of PGE and crystallization of PGM in natural sulfide melt.

6.1. Low proportions of PGE and semimetal elements in BMS

The proportions of PGE and semimetals in pyrrhotite, pentlandite and chalcopyrite from the Yangliuping sulfide ores were calculated following the method proposed by Barnes et al. (2006) (Fig. 9A). All the LA-ICPMS data (Table 4) used in the calculation are shown in the smooth spectra without PGE peaks, indicating that PGE hosted by the BMS as solid solution in our calculations (Fig. 5A-C). When the concentration of PGE was below the detection limits of LA-ICPMS analysis, detection limit values were used in calculation (Chen et al., 2015).

Our calculations indicate that < 40% Os, < 15% Ir and < 25% Pd are contained in the BMS, respectively, although almost 60% Ru is hosted in the BMS in the Yangliuping sulfide ores (Fig. 9A, Supplementary Table S2). In addition, percentages of Pt, Rh and semimetals hosted by the BMS are < 10%. The proportions of both PGE and semimetals in the BMS from the Yangliuping deposit are evidently lower than those in the BMS from the Jinchuan and Noril'sk deposits and slightly lower than those in the BMS from the Sudbury deposit (Figs. 9B, C, D) (Barnes et al., 2008; Dare et al., 2010b; Chen et al., 2015). Considering mass balance, the relatively low proportions of PGE in the BMS (Fig. 9A) imply that more PGE occur as discrete PGM phases or contained by CGSS at the Yangliuping deposit. This speculation is consistent with the occurrences of many micrometer- and nanometer-size PGM (Figs. 4, 5, 6, 8) and CGSS, which are enriched in Pd and Rh (Table 3) (Song et al., 2004).

Mineralogical evidence from natural ores as well as experimental evidence support a strong role of semimetals, especially As, on the distribution of PGE at magmatic temperatures (Gervilla et al., 1996; Pina et al., 2013). Experimental evidence shows that PGE-arsenides and sulfarsenides are all high temperatures phases and are likely to crystallize directly from sulfide and silicate melts (Kamenetsky et al., 2015;

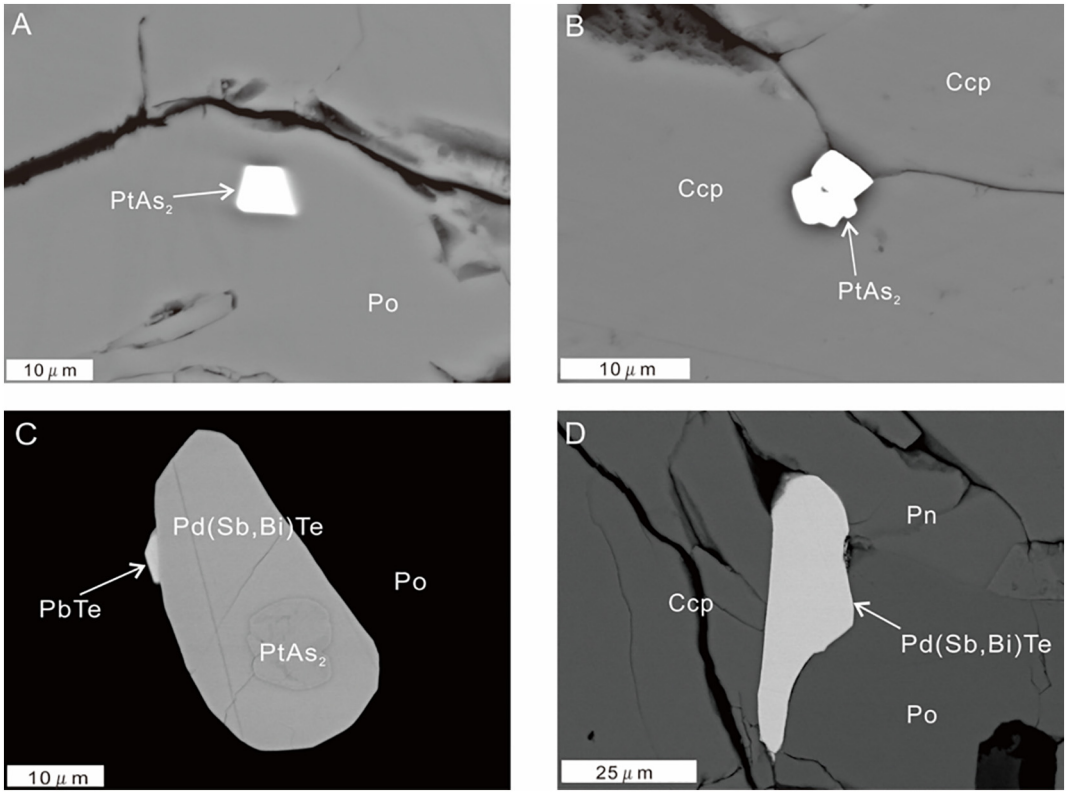

Fig. 7. Backscattered electron images of micrometer-size PGM. A. Euhedral sperrylite ($PtAs_2$) enclosed in pyrrhotite. B. Clusters of euhedral sperrylites in chalcopyrite. C. Anhedral testibiopalladite with a rounded sperrylite core, enclosed in pyrrhotite. A subhedral altaite on margin of the testibiopalladite. D. Anhedral testibiopalladite, located at the junction among pyrrhotite, pentlandite and chalcopyrite. Abbreviations: $PtAs_2$ = sperrylite, Ccp = chalcopyrite, Po = pyrrhotite, Pn = pentlandite. Pd(Sb, Bi)Te = testibiopalladite, PbTe = altaite.

Table 6
Numbers of nanometer-size PGE-arsenides and sulfarsenides and their host minerals identified in the massive and disseminated sulfide ores of the Yangliuping deposit.

Particle type	Host mineral				Total
	Pyrrhotite	Pentlandite	Chalcopyrite	CGSS	
Ir-Pt-AsS		1		1	2
Ir-Rh-AsS		2		9	11
Ir-Rh-Pt-AsS	10	5	1	9	25
Ir-Ru-Rh-Pt-AsS		1			1
Os-Ir-Rh-AsS				1	1
Os-Ir-Rh-Pt-AsS	4	4	4	2	14
Os-Ir-Rh-Pt-Pd-AsS		2			2
Os-Ir-Ru-AsS	1				1
Os-Ir-Ru-Rh-Pt-AsS	1	1			2
Os-Ir-Ru-Rh-Pt-Pd-AsS	3				3
Rh-AsS				8	8
Rh-Pt-AsS				4	4
$PtAs_2$	8	4	2		14
Total	27	20	7	34	

Maier et al., 2015). Additionally, all of the nanometer-size PGM discovered in the pyrrhotite and pentlandite as well as chalcopyrite are Os-Ir-Rh-Pt arsenides and sulfarsenides (Fig. 8, Table 6). Therefore, the low PGE proportions in the BMS are likely related to semimetals in the sulfide melt at Yangliuping. A basic question is what controls the proportions of semimetals in the BMS (Fig. 9) and whether the semimetal elements play a role in the distribution of PGE in the BMS in these deposits.

6.2. Formation of nanometer-size PGE-arsenides and sulfarsenides in BMS and CGSS

The nanometer-size PGM in the Yangliuping deposit have several prominent characteristics, which cannot be convincingly interpreted by crystallization from residual sulfide liquid at the last stage of solidification or subsolidus exsolution from BMS. First of all, the nanometer-size PGM comprising of arsenides and sulfarsenides of Os-Ir-Rh-Pt are not only found in the pyrrhotite, pentlandite but also in the chalcopyrite (Figs. 4, 5, 6, 8, Table 6). If the PGE-arsenides and sulfarsenides were formed by subsolidus solution of PGE from the BMS, those enclosed in the pyrrhotite and pentlandite should be more enriched in IPGE than those in the chalcopyrite. This is because IPGE are compatible with MSS, which exsolves pyrrhotite and pentlandite during cooling. Whereas, chalcopyrite is formed by exsolution from ISS, which is crystallized from residual sulfide liquid relatively depleted in IPGE. Secondly, the PGE-arsenides and sulfarsenides may form clusters in the core or mantle of the euhedral and chemically zoned CGSS grains, which were observed in the pyrrhotite and pentlandite as well as chalcopyrite (Fig. 4, Table 6) (Song et al., 2004). Thirdly, the nanometer-size PGE-arsenides and sulfarsenides are euhedral or subhedral and some of them show compositional zonation (Fig. 8). Such textural relationships indicate that the nanometer-size PGE-arsenides and sulfarsenides crystallized earlier than or concurrently with CGSS before crystallization of MSS. Noble metal-rich nanocrystals, as small as 30 nm, were also discovered in the pyrrhotite and pentlandite of the Merensky reef by high resolution transmission electron microscopy (HRTEM). No orientation relationship between the Ru-Rh-Pt-arsenide nanocrystals and the BMS matrix led Wirth et al. (2013) to conclude that they were formed prior to the crystallization of sulfides.

Arsenic is incompatible with MSS and tends to remain in sulfide liquid or form arsenide or sulfarsenide during MSS crystallization

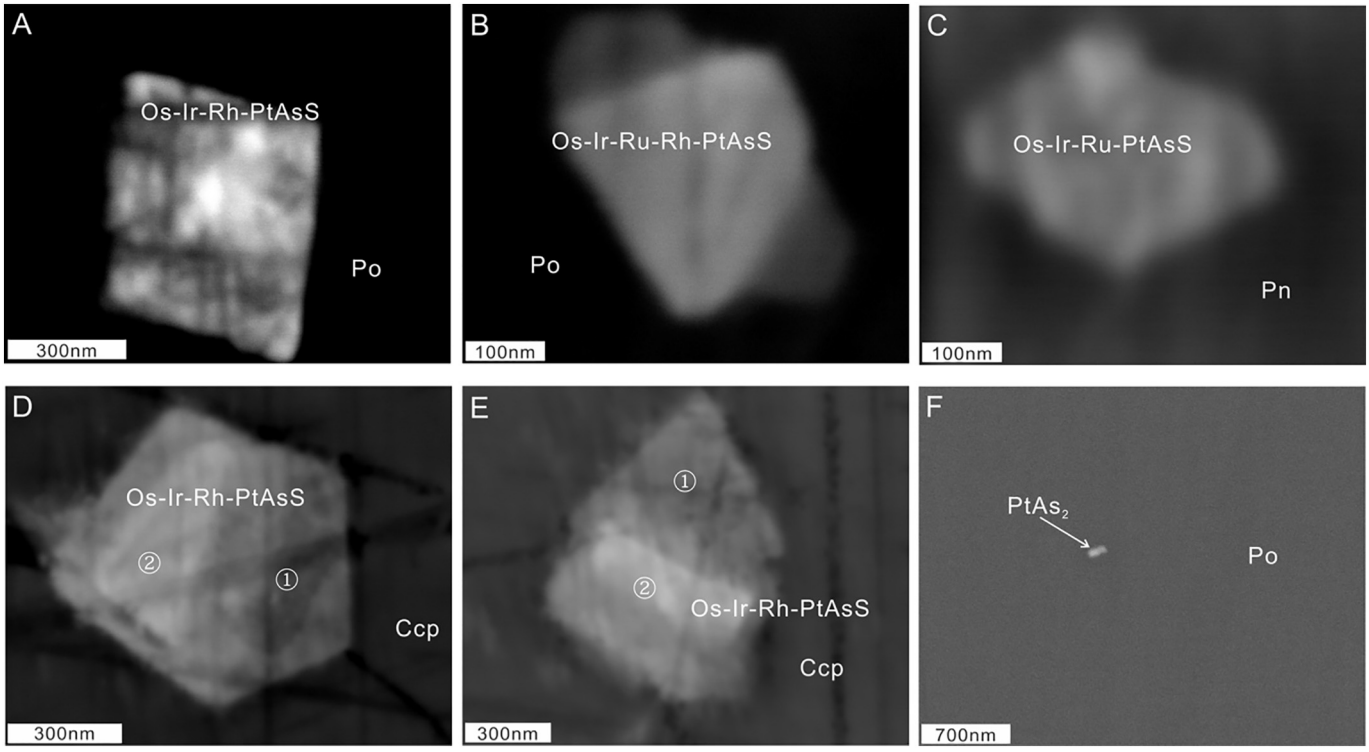

Fig. 8. Backscattered electron images of nanometer-size PGE-arsenides and sulfarsenides. A–E. Enhedral nanometer-size PGE-sulfarsenides enclosed in pyrrhotite, pentlandite and chalcopyrite. F. Nanometric sperrylite in pyrrhotite. Some nanometer-size PGE-sulfarsenides show obviously zoning texture (B, D, E). EDX analysis indicate that the rim (marked as ① in D and E) are higher in Co and Ni than the core (marked as ① in D and E). Abbreviations: Os-Ir-(Ru)-Rh-PtAsS = nanometer-size PGE sulfarsenides. Pn = pentlandite, Po = pyrrhotite, Ccp = chalcopyrite. $PtAs_2$ = sperrylite.

(Helmy et al., 2013a; Liu and Brenan, 2015). Partition coefficient of Pt between MSS and sulfide liquid evidently decreases due to an increase of As content in the sulfide liquid at 950 °C (Helmy et al., 2013b). Although supersaturation of PGE and As in the sulfide liquid is necessary for crystallization of PGE-arsenides according to classic nucleation theory, experiments by Helmy et al. (2013b) showed that Pt—As nanodroplets are stable as high as 1180C in a sulfide melt highly undersaturated with crystalline sperrylite. They proposed that cationic Pt and anionic As can form Pt—As molecular associations or polymolecular $(Pt—As)_n$ clusters, in this associated form, they are not substitutable in MSS via Fe substitution and exist in the form of nanometer-size As-enriched melt globules (Helmy et al., 2010; Helmy et al., 2013b). We propose that the nanometer-size PGE-arsenides and sulfarsenides enclosed in the BMS and CGSS of the Yangliuping deposit most likely formed very early due to the existence of PGE-As molecular or polymolecular clusters in the sulfide melt at high temperature. Relatively high contents of semimetal elements, particularly As, in the sulfide melt played an important role for the formation of the discrete nanometer-size PGE-arsenides and sulfarsenides before MSS crystallization in the Yangliuping deposit (Figs. 4, 8). This probably led to the depletion of the Yangliuping sulfides in PGE relative those in the Noril'sk, Jinchuan and Sudbury deposits (Fig. 9).

6.3. Solidification of the sulfide melt at Yangliuping

The above discussions allow us to propose an interpretation of the solidification processes of sulfide melt at Yangliuping. The occurrences of sperrylite, testibiopalladite and melonite (Song et al., 2004) and absence of magnetite in the Yangliuping sulfide ores demonstrate that the sulfide melt has moderate f_{S2} and As is predominantly anionic. Thus, associations and molecules between PGE and semimetals (with exception of Se, which has lower affinity with PGE than the other semimetals) could have formed in the sulfide melt at high temperature (Helmy and Bragagni, 2017; Helmy and Fonseca, 2017). The PGE-As molecules or polymolecular clusters could form relatively stable nanoparticles of Os-Ir-Rh-Pt sulfarsenides during cooling before the onset of MSS crystallization (Helmy et al., 2013b).

As a sulfarsenide, the CGSS probably crystallized following the nanometer-size PGE-arsenides, sulfarsenides and the MSS (Hansen et al., 1958; Bennett and Heyding, 1966; Helmy et al., 2013a). The PGE-arsenides or sulfarsenides in the cores of zoned CGSS probably formed due to the early formed PGE-arsenides or sulfarsenides were wetted by

Table 7
Numbers of micrometer-size CGSS, PGM and their texture relationships identified in the Yangliuping deposit.

Host mineral	Cobaltite-gersdorffite solid solution (CGSS)	Sperrylite ($PtAs_2$)	PGE sulfarsenide (IrRhPt)AsS	testibiopalladite $Pd(Te,Sb,Bi)_2$	Pd melonite $(Pd,Ni)(Bi,Te)_2$
Po	66	11		3	2
Pn	6	2			1
Ccp	12	8			
CGSS		2	1		
$Pd(Te,Sb,Bi)_2$		1			
BMS/BMS boundary	6			2	1
Total	90	24	1	5	4

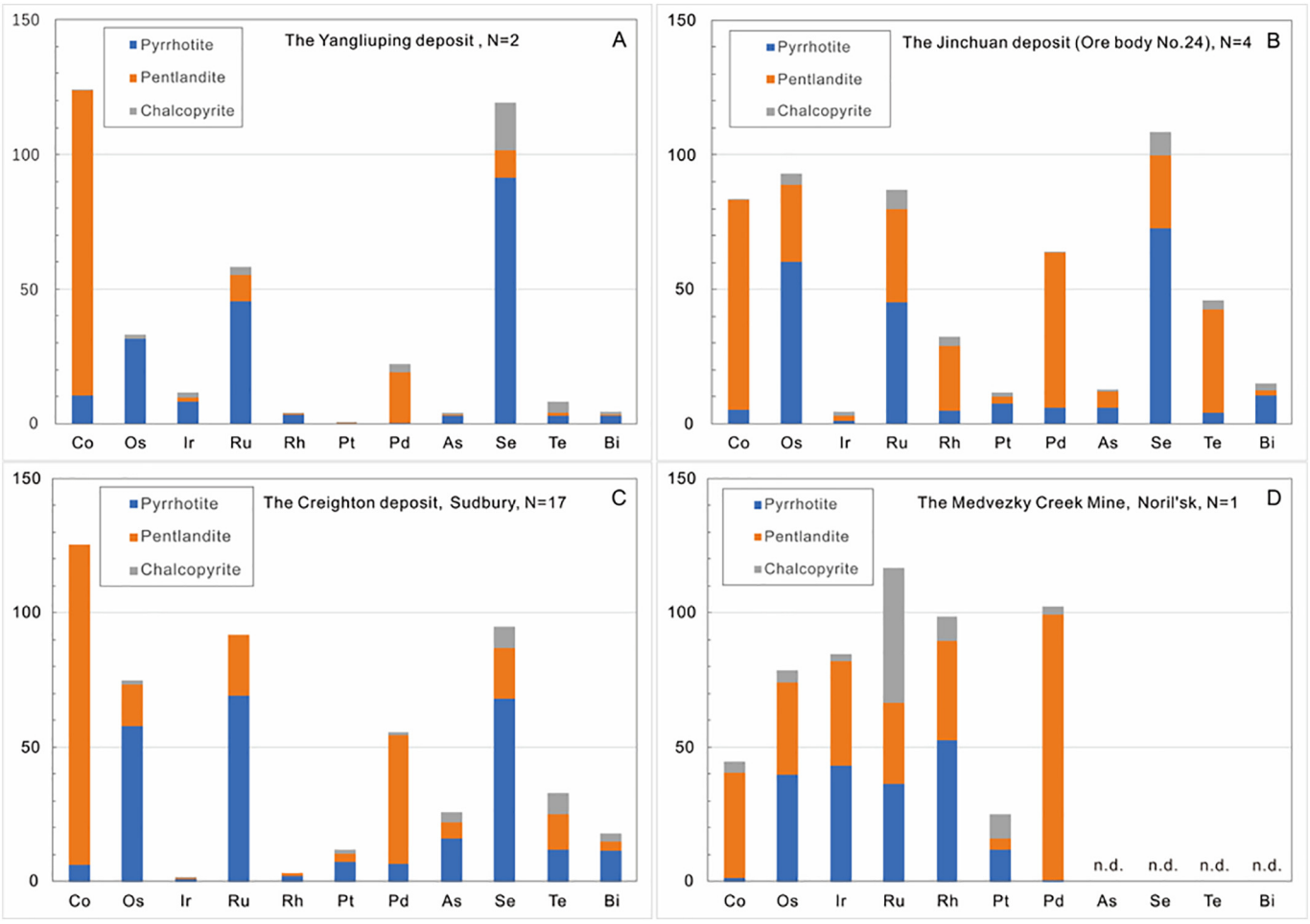

Fig. 9. Mass balance of PGE, chalcophile and semimetal elements in BMS from (A) the Yangliuping deposit (this study), (B) the Jinchuan deposit (Chen et al., 2013; Chen et al., 2015), (C) the Creighton deposit, Sudbury (Dare et al., 2010a) and (D) the Medvezhiy Creek Mine, Noril'sk (Barnes et al., 2008). Plotted as proportion of each element in pyrrhotite (Po), pentlandite (Pn) and chalcopyrite (Ccp). N: number of samples analyzed, n.d. = not detected.

immiscible Ni-Co-arsenide melt, which was later crystallized to CGSS. Thus, the CGSS not only enclosed plenty of the discrete and cluster of nanometer-size PGE-arsenides and sulfarsenides but also formed PGE-rich cores and Co-rich rims and have euhedral shapes (Song et al., 2004). The discrete nanometer-size PGE-arsenides and sulfarsenides distributed in the sulfide melt were also enclosed by MSS and ISS. This inference is supported by the experimental observation that euhedral PGE-sulfarsenides were enclosed by MSS and ISS (Helmy and Bragagni, 2017). Then, the nanometer-size PGE-arsenides and sulfarsenides with similar compositions became inclusions in pyrrhotite, pentlandite and chalcopyrite due to subsolid exsolution of MSS and ISS during cooling. The early formation of the nanometer-size PGE-arsenides and sulfarsenides partly prevented PGE and As to enter MSS as solid solution and resulted in the low proportions of PGE and As in the BMS at Yangliuping (Fig. 9A). Because Pd does not form high temperature phases with semimetals (Helmy et al., 2007, 2013a; Helmy and Bragagni, 2017), it partitions into a melt phase; likely it stayed in the sulfide melt or partitions into an immiscible semimetal melt (e.g. Holwell and McDonald, 2007; Helmy et al., 2007). The high Pd content of pentlandite is more likely the result of diffusion of Pd from surrounding residual liquid during subsolidus exsolution of pentlandite from MSS (Barnes et al., 2006; Chen et al., 2015). Such a process caused the cores of pentlandite to be richer in Pd than the margins (Fig. 6H). Similar phenomenon was observed in the Creighton Ni—Cu-PGE sulfide deposit, Sudbury (Dare et al., 2010a).

Experiments indicated that Te, Bi and Sb are highly incompatible and As is moderate incompatible with MSS (Helmy et al., 2013a; Liu and Brenan, 2015). In theory, very low solubility of semimetals in MSS rules out that any discrete antimonide, telluride, or bismuthinide phases in magmatic sulfides are interpreted as subsolidus exsolution (Ballhaus and Ulmer, 1995). Growth of the micrometer-size PGM at the boundary between BMS or at the margins of BMS (Fig. 7) may have continued to low temperature. Sperrylite formed at high temperature (Helmy et al., 2013b) and the others, such as testibiopalladite, probably crystallized from the residual liquid at relatively low temperature.

7. Conclusion

In the Yangliuping Ni—Cu-PGE sulfide deposit, PGE exist in the base metal sulfides as both solid solution and nanometer-size PGE-arsenides and sulfarsenides. Pentlandite is most enriched in Pd, pyrrhotite is relatively enriched in Os, whereas chalcopyrite is relatively barren in PGE (Table 4). The euhedral nanometer-size Os-Ir-Rh-Pt arsenides and sulfarsenides not only occur in CGSS, pyrrhotite and pentlandite, but also in chalcopyrite. This demonstrated early crystallization of nanometer-size PGE-arsenides and sulfarsenides at high temperature due to the existence of PGE-As molecular or polymolecular clusters in the sulfide melt. Arsenic plays an important role in the formation of the nanometer-size PGE-arsenides and sulfarsenides.

Acknowledgements

This work was supported by NSFC projects of China (41473050, 41630316 and 41772067 to X.-Y. Song), National Key Research and

Development Program of China (2016YFC0600503) and Open Funding Project of State Key Laboratory for Mineral Deposits Research, Nanjing University (2018-LAMD-K08). We greatly appreciate Steve Barnes, Marina Yudovskya and Dan Zhu for their constructive discussions. We also thank the assistance of Sai-Hong Yang, Wen-Lan Zhang and Shao-Hua Dong during the measurements, and Sheng-Hua Zhou during the fieldwork.

Appendix A. Supplementary data

Supplementary data to this article can be found online at https://doi.org/10.1016/j.chemgeo.2019.04.015.

References

Bai, L.P., Barnes, S.-J., Baker, D.R., 2017. Sperrylite saturation in magmatic sulfide melts: Implications for formation of PGE-bearing arsenides and sulfarsenides. Am. Mineral. 102 (5), 966–974. https://doi.org/10.2138/am-2017-5631.

Ballhaus, C., Sylvester, P., 2000. Noble metal enrichment processes in the Merensky Reef, Bushveld Complex. J. Petrol. 41 (4), 545–561. https://doi.org/10.1093/petrology/41.4.545.

Ballhaus, C., Ulmer, P., 1995. Platinum-group elements in the Merensky Reef: II. Experimental solubilities of platinum and palladium in $Fe_{1-x}S$ from 950 to 450°C under controlled f_{S2} and f_{H2}. Geochim. Cosmochim. Acta 59 (23), 4881–4888 (doi:10.1016/0016-7037(95)00355-x).

Ballhaus, C., Tredoux, M., Spath, A., 2001. Phase relations in the Fe-Ni-Cu-PGE-S system at magmatic temperature and application to massive sulphide ores of the Sudbury Igneous Complex. J. Petrol. 42 (10), 1911–1926. https://doi.org/10.1093/petrology/42.10.1911.

Barnes, S.J., Lightfoot, P.C., 2005. Formation of magmatic nickel sulfide ore deposits and processes affecting their copper and platinum group element contents. Econ. Geol. 100, 179–213.

Barnes, S., Maier, W.D., 1999. The fractionation of Ni, Cu and the noble metals in silicate and sulphide liquids. In: Keays, R.R., Lesher, C.M., Lightfoot, P.C., Farrow, C.E.G. (Eds.), Dynamic Processes in Magmatic Ore Deposits and their Application in Mineral Exploration. Geological Association of Canada, Newfoundland, pp. 69–106.

Barnes, S.-J., Makovicky, E., Makovicky, M., Rose-Hansen, J., Karup-Moller, S., 1997. Partition coefficients for Ni, Cu, Pd, Pt, Rh, and Ir between monosulfide solid solution and sulfide liquid and the formation of compositionally zoned Ni–Cu sulfide bodies by fractional crystallization of sulfide liquid. Can. J. Earth Sci. 34 (4), 366–374. https://doi.org/10.1139/e17-032.

Barnes, S.-J., van Achterbergh, E., Makovicky, E., Li, C., 2001. Proton microprobe results for the partitioning of platinum-group elements between monosulphide solid solution and sulphide liquid. S. Afr. J. Geol. 104 (4), 275–286. https://doi.org/10.2113/104.4.275.

Barnes, S.-J., Cox, R.A., Zientek, M.L., 2006. Platinum-group element, gold, silver and base metal distribution in compositionally zoned sulfide droplets from the Medvezky Creek Mine, Noril'sk, Russia. Contrib. Mineral. Petrol. 152 (2), 187–200. https://doi.org/10.1007/s00410-006-0100-9.

Barnes, S.-J., Prichard, H.M., Cox, R.A., Fisher, P.C., Godel, B., 2008. The location of the chalcophile and siderophile elements in platinum-group element ore deposits (a textural, microbeam and whole rock geochemical study): Implications for the fortnation of the deposits. Chem. Geol. 248 (3–4), 295–317. https://doi.org/10.1016/j.chemgeo.2007.08.004.

Bennett, S., Heyding, R., 1966. Arsenides of the transition metals: viii. some binary and ternary group viii diarsenides and their magnetic and electrical properties. Can. J. Chem. 44 (24), 3017–3030. https://doi.org/10.1139/v66-444.

Brenan, J.M., 2002. Re-Os fractionation in magmatic sulfide melt by monosulfide solid solution. Earth Planet. Sci. Lett. 199 (3–4), 257–268. https://doi.org/10.1016/S0012-821x(02)00581-2.

Cabri, L.J., 2002. The platinum-group minerals. In: Cabri, L.J. (Ed.), The Geology, Geochemistry, Mineralogy and Mineral Beneficiation of Platinum-Group Elements. vol. special volume 54. Canadian Institute of Mining, Metallurgy and Petroleum, Calgary, pp. 13–129.

Cabri, L.J., Laflamme, J.H.G., 1976. The mineralogy of the platinum-group elements from some copper-nickel deposits of the Sudbury area, Ontario. Econ. Geol. 71, 1159–1195. https://doi.org/10.2113/gsecongeo.71.7.1159.

Cabri, L.J., Rudashevsky, N.S., Rudashevsky, V.N., 2008. Current approaches for the process mineralogy of platinum-group element ores and tailings. In: Ninth International Congress for Applied Mineralogy ICAM 2008. The Australasian Institute of Mining and Metallurgy, pp. 9–17 Publication Series No 8/2008.

Cabri, L.J., Kelvin, M., Yang, Z., Jackson, S.E., Altun, O., 2017. Application of LA-ICP-MS trace-element analysis for precious metal deportment: a case study of the Kevitsa mine, Finland. Eur. J. Mineral. 29, 635–644. https://doi.org/10.1127/ejm/2017/0029-2644.

Canali, A., Brenan, J., Sullivan, N., 2017. Solubility of platinum-arsenide melt and sperrylite in synthetic basalt at 0.1 MPa and 1200°C with implications for arsenic speciation and platinum sequestration in mafic igneous systems. Geochim. Cosmochim. Acta 216, 153–168. https://doi.org/10.1016/j.gca.2017.05.006.

Chen, L.M., Song, X.Y., Keays, R.R., Tian, Y.L., Wang, Y.S., Deng, Y.F., Xiao, J.F., 2013. Segregation and fractionation of magmatic Ni-Cu-PGE sulfides in the Western Jinchuan Intrusion, Northwestern China: insights from Platinum Group Element Geochemistry. Econ. Geol. 108 (8), 1793–1811. https://doi.org/10.2113/econgeo.108.8.1793.

Chen, L.-M., Song, X.-Y., Danyushevsky, L.V., Wang, Y.-S., Tian, Y.-L., Xiao, J.-F., 2015. A laser ablation ICP-MS study of platinum-group and chalcophile elements in base metal sulfide minerals of the Jinchuan Ni–Cu sulfide deposit, NW China. Ore Geol. Rev. 65, 955–967. https://doi.org/10.1016/j.oregeorev.2014.07.011.

Chung, S.L., Jahn, B.M., 1995. Plume-lithosphere interaction in generation of the Emeishan Flood Basalts at the Permian-Triassic Boundary. Geology 23 (10), 889–892. https://doi.org/10.1130/0091-7613(1995)023<0889:Pliigo>2.3.Co;2.

Czamanske, G.K., Kunilov, V.E., Zientek, M.L., Cabri, L.J., Calk, L.C., Likhachev, A.P., 1992. A proton-microprobe study of sulfide ores from the Noril'sk-Talnakh district, Siberia. Can. Mineral. 30, 249–287.

Danyushevsky, L., Robinson, P., Gilbert, S., Norman, M., Large, R., McGoldrick, P., Shelley, M., 2011. Routine quantitative multi-element analysis of sulphide minerals by laser ablation ICP-MS: Standard development and consideration of matrix effects. Geochemistry-Exploration Environment Analysis 11 (1), 51–60. https://doi.org/10.1144/1467-7873/09-244.

Dare, S.A.S., Barnes, S.J., Prichard, H.M., 2010a. The distribution of platinum group elements (PGE) and other chalcophile elements among sulfides from the Creighton Ni–Cu–PGE sulfide deposit, Sudbury, Canada, and the origin of palladium in pentlandite. Mineral. Deposita 45 (8), 765–793. https://doi.org/10.1007/s00126-010-0295-6.

Dare, S.A.S., Barnes, S.J., Prichard, H.M., Fisher, P.C., 2010b. The timing and formation of platinum-group minerals from the Creighton Ni-Cu-Platinum-Group Element Sulfide Deposit, Sudbury, Canada: early Crystallization of PGE-Rich Sulfarsenides. Econ. Geol. 105 (6), 1071–1096. https://doi.org/10.2113/econgeo.105.6.1071.

Duran, C., Barnes, S., Pleše, P., Prašek, M.K., Zientek, M., Pagé, P., 2017. Fractional crystallization-induced variations in sulfides from the Noril'sk-Talnakh mining district (polar Siberia, Russia). Ore Geol. Rev. 90, 326–351. https://doi.org/10.1016/j.oregeorev.2017.05.016.

Fleet, M.E., Chryssoulis, S.L., Stone, W.E., Weisener, C.G., 1993. Partitioning of platinum-group elements and Au in the Fe−Ni−Cu−S system: experiments on the fractional crystallization of sulfide melt. Contrib. Mineral. Petrol. 115 (1), 36–44.

Gervilla, F., Leblanc, M., Torres-Ruiz, J., Hach-Ali, P.F., 1996. Immiscibility between arsenide and sulfide melts; a mechanism for concentration of noble metals. Can. Mineral. 34 (3), 485–502.

Gilbert, S., Danyushevsky, L., Robinson, P., Wohlgemuth-Ueberwasser, C., Pearson, N., Savard, D., Norman, M., Hanley, J., 2013. A comparative study of five reference materials and the Lombard meteorite for the determination of the platinum-group elements and gold by LA-ICP-MS. Geostand. Geoanal. Res. 37 (1), 51–64. https://doi.org/10.1111/j.1751-908X.2012.00170.x.

Godel, B., Barnes, S.-J., 2008. Image analysis and composition of platinum-group minerals in the JM Reef, Stillwater Complex. Econ. Geol. 103 (3), 637–651. https://doi.org/10.2113/gsecongeo.103.3.637.

Godel, B., Barnes, S.J., Maier, W.D., 2007. Platinum-group elements in sulphide minerals, platinum-group minerals, and whole-rocks of the Merensky Reef (Bushveld Complex, South Africa): implications for the formation of the reef. J. Petrol. 48 (8), 1569–1604. https://doi.org/10.1093/petrology/egm030.

Godel, B., Barnes, S.J., Barnes, S.-J., Maier, W.D., 2010. Platinum ore in three dimensions: Insights from high-resolution X-ray computed tomography. Geology 38 (12), 1127–1130. https://doi.org/10.1130/G31265.1.

Hanley, J.J., 2007. The role of arsenic-rich melts and mineral phases in the development of high-grade Pt-Pd mineralization within komatiite-associated magmatic Ni-Cu sulfide horizons at dundonald beach south, Abitibi subprovince, Ontario, Canada. Econ. Geol. 102 (2), 305–317. https://doi.org/10.2113/gsecongeo.102.2.305.

Hansen, M., Anderko, K., Salzberg, H., 1958. Constitution of binary alloys. J. Electrochem. Soc. 105 (12), 260C–261C.

Helmy, H.M., Bragagni, A., 2017. Platinum-group elements fractionation by selective complexing, the Os, Ir, Ru, Rh-arsenide-sulfide systems above 1020°C. Geochim. Cosmochim. Acta 216, 169–183. https://doi.org/10.1016/j.gca.2017.01.040.

Helmy, H.M., Fonseca, R.O.C., 2017. The behavior of Pt, Pd, Cu and Ni in the Se-sulfide system between 1050 and 700°C and the role of Se in platinum-group elements fractionation in sulfide melts. Geochim. Cosmochim. Acta 216, 141–152. https://doi.org/10.1016/j.gca.2017.05.010.

Helmy, H.M., Ballhaus, C., Berndt, J., Bockrath, C., Wohlgemuth-Ueberwasser, C., 2007. Formation of Pt, Pd and Ni tellurides: experiments in sulfide–telluride systems. Contrib. Mineral. Petrol. 153 (5), 577–591.

Helmy, H.M., Ballhaus, C., Wohlgemuth-Ueberwasser, C., Fonseca, R.O.C., Laurenz, V., 2010. Partitioning of Se, As, Sb, Te and Bi between monosulfide solid solution and sulfide melt — application to magmatic sulfide deposits. Geochim. Cosmochim. Acta 74 (21), 6174–6179. https://doi.org/10.1016/j.gca.2010.08.009.

Helmy, H., Ballhaus, C., Fonseca, R., Nagel, T., 2013a. Fractionation of platinum, palladium, nickel, and copper in sulfide–arsenide systems at magmatic temperature. Contrib. Mineral. Petrol. 166 (6), 1725–1737. https://doi.org/10.1007/s00410-013-0951-9.

Helmy, H.M., Ballhaus, C., Fonseca, R.O., Wirth, R., Nagel, T., Tredoux, M., 2013b. Noble metal nanoclusters and nanoparticles precede mineral formation in magmatic sulphide melts. Nat. Commun. 4, 2405. https://doi.org/10.1038/ncomms3405.

Holwell, D.A., McDonald, I., 2007. Distribution of platinum-group elements in the Platreef at Overysel, northern Bushveld Complex: a combined PGM and LA-ICP-MS study. Contrib. Mineral. Petrol. 154 (2), 171–190. https://doi.org/10.1007/s00410-007-0185-9.

Hutchinson, D., McDonald, I., 2008. Laser ablation ICP-MS study of platinum-group elements in sulphides from the Platreef at Turfspruit, northern limb of the Bushveld Complex, South Africa. Mineral. Deposita 43 (6), 695–711. https://doi.org/10.1007/

s00126-008-0190-6.
Kamenetsky, V.S., Park, J.W., Mungall, J.E., Pushkarev, E.V., Ivanov, A.V., Kamenetsky, M.B., Yaxley, G.M., 2015. Crystallization of platinum-group minerals from silicate melts: evidence from Cr-spinel-hosted inclusions in volcanic rocks. Geology 43 (10), 903–906. https://doi.org/10.1130/G37052.1.
Kosler, J., 2001. Laser-ablation ICPMS study of metamorphic minerals and processes. In: Sylvester, P.J. (Ed.), Laser-Ablation-ICPMS in the Earth Sciences: Principles and Applications. Mineralogical Association of Canada Short Course Handbook, Ottawa, pp. 185–202.
Liu, Y.N., Brenan, J., 2015. Partitioning of platinum-group elements (PGE) and chalcogens (Se, Te, As, Sb, Bi) between monosulfide-solid solution (MSS), intermediate solid solution (ISS) and sulfide liquid at controlled fO(2)-fS(2) conditions. Geochim. Cosmochim. Acta 159, 139–161. https://doi.org/10.1016/j.gca.2015.03.021.
Longerich, H.P., Jackson, S.E., Günther, D., 1996. Inter-laboratory note. Laser ablation inductively coupled plasma mass spectrometric transient signal data acquisition and analyte concentration calculation. J. Anal. At. Spectrom. 11 (9), 899–904. https://doi.org/10.1039/JA9961100899.
Maier, W.D., Rasmussen, B., Fletcher, I.R., Godel, B., Barnes, S.J., Fisher, L.A., Yang, S.H., Huhma, H., Lahaye, Y., 2015. Petrogenesis of the ~2·77 Ga Monts de Cristal complex, Gabon: evidence for direct precipitation of Pt-arsenides from basaltic magma. J. Petrol. 56 (7), 1285–1308. https://doi.org/10.1093/petrology/egv035.
Makovicky, E., 2002. Ternary and quaternary phase systems with PGE. In: Cabri, L.J. (Ed.), Geology, Geochemistry, Mineralogy and Mineral Beneficiation of Platinum-Group Elements. Canadian Institute of Mining, Metallurgy and Petroleum, Calgary, pp. 131–175.
Makovicky, E., Karup-Møller, S., 2000. Phase relations in the metal-rich portions of the phase system Pt-Ir-Fe-S at 1000°C and 1100°C. Mineral. Mag. 64 (6), 1047–1056. https://doi.org/10.1180/002646100550047.
Makovicky, M., Makovicky, E., Rose-Hansen, J., Gallagher, M.J., Ixer, R.A., Neary, C.R., Prichard, Margaret, H., 1986. Experimental studies on the solubility and distribution of platinum group elements in base-metal sulphides in platinum deposits. In: Metallogeny of Basic and Ultrabasic Rocks. The Institution of Mining and Metallurgy, London, pp. 415–425.
Mungall, J.E., Andrews, D.R.A., Cabri, L.J., Sylvester, P.J., Tubrett, M., 2005. Partitioning of Cu, Ni, Au, and platinum-group elements between monosulfide solid solution and sulfide melt under controlled oxygen and sulfur fugacities. Geochim. Cosmochim. Acta 69 (17), 4349–4360. https://doi.org/10.1016/j.gca.2004.11.025.
O'Driscoll, B., González-Jiménez, J.M., 2016. Petrogenesis of the platinum-group minerals. In: Harney, Jason, Day, Jarnes M.D. (Eds.), Reviews in Mineralogy and Geochemistry. Mineralogical Society of America, Chantilly, pp. 489–578.
Pina, R., Gervilla, F., Barnes, S.J., Ortega, L., Lunar, R., 2013. Partition coefficients of platinum group and chalcophile elements between arsenide and sulfide phases as determined in the beni bousera Cr-Ni mineralization (North Morocco). Econ. Geol. 108 (5), 935–951.
Power, M.R., Pirrie, D., Jedwab, J., Stanley, C.J., 2004. Platinum-group element mineralization in an As-rich magmatic sulphide system, Talnotry, southwest Scotland. Mineral. Mag. 68 (2), 395–411. https://doi.org/10.1180/0026461046820194.
Prichard, H.M., Hutchinson, D., Fisher, P.C., 2004. Petrology and crystallization history of multiphase sulfide droplets in a Mafic Dike from Uruguay: Implications for the origin of Cu-Ni-PGE sulfide deposits. Econ. Geol. 99 (2), 365–376. https://doi.org/10.2113/99.2.365.
Song, X.Y., 2004. Geochemistry of Permian Flood Basalts and Related Ni-Cu-(Pge) Sulfide-Bearing Sills in Yangliuping, Sichuan Province, China. Unpublished PhD thesis. The University of Hong Kong, Hong Kong.
Song, X.Y., Zhou, M.F., Hou, Z.Q., Cao, Z.M., Wang, Y.L., Li, Y.G., 2001. Geochemical constraints on the mantle source of the upper permian Emeishan continental flood basalts, southwestern China. Int. Geol. Rev. 43 (3), 213–225. https://doi.org/10.1080/00206810109465009.
Song, X.Y., Zhou, M.F., Cao, Z.M., Sun, M., Wang, Y.L., 2003. Ni-Cu-(PGE) magmatic sulfide deposits in the Yangliuping area, Permian Emeishan Igneous province, SW China. Mineral. Deposita 38 (7), 831–843. https://doi.org/10.1007/s00126-003-0362-3.
Song, X.Y., Zhou, M.F., Cao, Z.M., 2004. Genetic relationships between base-metal sulfides and platinum-group minerals in the Yangliuping Ni-Cu-(PGE) sulfide deposit, southwestern China. Can. Mineral. 42, 469–483. https://doi.org/10.2113/gscanmin.42.2.469.
Song, X.Y., Zhou, M.F., Keays, R.R., Cao, Z.M., Sun, M., Qi, L., 2006. Geochemistry of the Emeishan flood basalts at Yangliuping, Sichuan, SW China: implications for sulfide segregation. Contrib. Mineral. Petrol. 152 (1), 53–74. https://doi.org/10.1007/s00410-006-0094-3.
Song, X.Y., Zhou, M.F., Tao, Y., Xiao, J.F., 2008. Controls on the metal compositions of magmatic sulfide deposits in the Emeishan large igneous province, SW China. Chem. Geol. 253 (1–2), 38–49. https://doi.org/10.1016/j.chemgeo.2008.04.005.
Song, X.Y., Qi, H.W., Hu, R.Z., Chen, L.M., Yu, S.Y., Zhang, J.F., 2013. Formation of thick stratiform Fe-Ti oxide layers in layered intrusion and frequent replenishment of fractionated mafic magma: evidence from the Panzhihua intrusion, SW China. Geochem. Geophys. Geosist. 14 (3), 712–732. https://doi.org/10.1002/ggge.20068.
Sylvester, P.J., Cabri, L.J., Tubrett, M.N., McMahon, G., Laflamme, J.H.G., Peregoedova, A., 2005. Synthesis and evaluation of a fused pyrrhotite standard reference material for platinum group element and gold analysis by laser ablation–ICPMS. In: Tormanen, T.O., Alapieti, T.T. (Eds.), 10th International Platinum Symposium "Platinum Group Elements — From Genesis to Beneficiation and Environmental Impact", Oulu, Finland, pp. 16–20.
Tao, Y., et al., 2007. Petrogenesis of the Pt-Pd mineralized Jinbaoshan ultramafic intrusion in the Permian Emeishan Large Igneous Province, SW China. Contrib. Mineral. Petrol. 153 (3), 321–337. https://doi.org/10.1007/s00410-006-0149-5.
Tao, Y., Li, C., Song, X.-Y., Ripley, E.M., 2008. Mineralogical, petrological, and geochemical studies of the Limahe mafic–ultramatic intrusion and associated Ni–Cu sulfide ores, SW China. Miner. Depos. 43 (8), 849–872. https://doi.org/10.1007/s00126-008-0207-1.
Tarkian, M., Prichard, H.M., 1987. Irarsite-hollingworthite solid-solution series and other associated Ru-, Os-, Ir-, and Rh-bearing PGM's from the Shetland ophiolite complex. Miner. Depos. 22 (3), 178–184.
Tomkins, A.G., 2010. Wetting facilitates late-stage segregation of precious metal–enriched sulfosalt melt in magmatic sulfide systems. Geology 38 (10), 951–954. https://doi.org/10.1130/G31263.1.
Wirth, R., Reid, D., Schreiber, A., 2013. Nanometer-sized platinum-group minerals (PGM) in base metal sulfides: New evidence for an orthomagmatic origin of the Merensky Reef PGE ore deposit, Bushveld Complex, South Africa. Can. Mineral. 51 (1), 143–155. https://doi.org/10.3749/canmin.51.1.143.
Xu, Y., Chung, S.-L., Jahn, B.-m., Wu, G., 2001. Petrologic and geochemical constraints on the petrogenesis of Permian–Triassic Emeishan flood basalts in southwestern China. Lithos 58 (3–4), 145–168. https://doi.org/10.1016/s0024-4937(01)00055-x.
Zelenski, M., Kamenetsky, V.S., Mavrogenes, J.A., Danyushevsky, L.V., Matveev, D., Gurenko, A.A., 2017. Platinum-group elements and gold in sulfide melts from modern arc basalt (Tolbachik volcano, Kamchatka). Lithos 290-291, 172–188. https://doi.org/10.1016/j.lithos.2017.08.012.
Zhong, H., Zhou, X.H., Zhou, M.F., Sun, M., Liu, B.G., 2002. Platinum-group element geochemistry of the Hongge Fe-V-Ti deposit in the Pan-Xi area, southwestern China. Mineral. Deposita 37 (2), 226–239. https://doi.org/10.1007/s00126-001-0220-0.
Zhou, M.-F., Yang, Z., Song, X., Lesher, C., Keays, R., 2002. Magmatic Ni-Cu-(PGE) sulfide deposits in China. In: Cabri, L.J. (Ed.), The Geology, Geochemistry, Mineralogy, Mineral Benification of Platinum-Group Elements. Canadian Institute of Mining, Metallurgy and Petroleum, Calgary, pp. 619–636.
Zientek, M.L., Likhachev, A.P., Kunilov, V.E., Barnes, S.J., Meier, A.L., Carlson, R.R., Briggs, P.H., Fries, T.L., Adrian, B.M., Lightfoot, P.C., 1994. Cumulus processes and the composition of magmatic ore deposits: Examples from the Talnakh District, Russia. In: Proceedings of the Sudbury - Noril'sk Symposium Special. vol. 5. pp. 373–392.